For Reference

NOT TO BE TAKEN FROM THIS ROOM

Thesis
1969(F)
30

For Reference

NOT TO BE TAKEN FROM THIS ROOM

Ex libris
universitatis
albertaensis

The University of Alberta
Printing Department
Edmonton, Alberta

UNIVERSITY OF ALBERTA
LIBRARY

Regulations Regarding Theses and Dissertations

Typescript copies of theses and dissertations for Master's and Doctor's degrees deposited in the University of Alberta Library, as the official Copy of the Faculty of Graduate Studies, may be consulted in the Reference Reading Room only.

A second copy is on deposit in the Department under whose supervision the work was done. Some Departments are willing to loan their copy to libraries, through the inter-library loan service of the University of Alberta Library.

These theses and dissertations are to be used only with due regard to the rights of the author. Written permission of the author and of the Department must be obtained through the University of Alberta Library when extended passages are copied. When permission has been granted, acknowledgement must appear in the published work.

This thesis or dissertation has been used in accordance with the above regulations by the persons listed below. The borrowing library is obligated to secure the signature of each user.

Please sign below:

Date	Signature	Institution

THE UNIVERSITY OF ALBERTA

GENERATION OF A CLEAN (III) COPPER SURFACE

by

© LORNE GRANT BROWN

A THESIS

SUBMITTED TO THE FACULTY OF GRADUATE STUDIES

IN PARTIAL FULFILMENT OF THE REQUIREMENTS FOR THE DEGREE

OF MASTER OF SCIENCE

DEPARTMENT OF MECHANICAL ENGINEERING

EDMONTON, ALBERTA

FALL, 1969

UNIVERSITY LIBRARY
UNIVERSITY OF ALBERTA

Thesis
1969(F)
30

UNIVERSITY OF ALBERTA

FACULTY OF GRADUATE STUDIES

The undersigned certify that they have read, and recommend to the Faculty of Graduate Studies for acceptance, a thesis entitled "Generation of a Clean (III) Copper Surface" submitted by Lorne Grant Brown in partial fulfilment of the requirements for the degree of Master of Science.

UNIVERSITY OF ALBERTA

FACULTY OF GRADUATE STUDIES

The undersigned certify that they have read, and recommend to the Faculty of Graduate Studies for acceptance, a thesis entitled "Generation of a Clean (111) Copper Surface" submitted by Lorne Grant Brown in partial fulfillment of the requirements for the degree of Master of Science.

ABSTRACT

The diffraction pattern of a clean, well ordered, (III) plane of a single copper crystal was obtained by heating the crystal for 200 hours at 1000°F followed by 50 hours heating at 1500-1600°F. The work function change of the initially degassed surface (200 hours heating at 1000°F) after 50 hours heating at 1500-1600°F was +0.55 electron volts. Additional heating for 350 hours at 1500-1600°F changed the work function of the clean surface by -0.40 electron volts.

An oxygen exposure of 3.8×10^{-5} torr-sec resulted in a work function change of +0.6 electron volts from that of the clean surface.

Nitrogen and hydrogen exposures did not change the surface work function.

ABSTRACT

The diffraction pattern of a clean, well ordered, (111) plane of a single copper crystal was obtained by heating the crystal for 200 hours at 1000°F followed by 50 hours heating at 1500-1600°F. The work function change of the initially degassed surface (200 hours heating at 1000°F) after 50 hours heating at 1500-1600°F was +0.55 electron volts. Additional heating for 350 hours at 1500-1600°F changed the work function of the clean surface by -0.40 electron volts.

An oxygen exposure of 3.8×10^{-5} torr-sec resulted in a work function change of +0.6 electron volts from that of the clean surface.

Nitrogen and hydrogen exposures did not change the surface work function.

ACKNOWLEDGEMENTS

The author wishes to extend his appreciation to:

- Dr. Marsden for his supervision of this thesis.
- Dr. Schmidt-Weinmar for his assistance throughout the entire project.
- Dr. Vitovec and Mr. Scott for their assistance in the sample preparation.
- The members of the Mechanical Engineering Shop for their cooperation, particularly Mr. H. Golls who built the apparatus.
- Helen Wozniuk for her patience in typing this thesis.
- The National Research Council for the funds made available under Grant No. A-2938.

TABLE OF CONTENTS

LIST OF TABLES

LIST OF FIGURES

CHAPTER I

INTRODUCTION

The study of gas-solid surface interactions has become important in recent years, with applications to aerodynamics of space vehicles, semi-conductors, catalytic processes, and many other instances where the properties of the solid surface are important.

One of the most difficult problems to be overcome in any experimental investigation of gas-solid surface interactions is that of obtaining a well specified solid surface. This is a two-fold problem involving methods of cleaning the surface and the instrumentation necessary to monitor the cleaning process.

Surface cleaning methods include resistive heating, electron bombardment, ion bombardment, and oxygen-hydrogen reduction. The instrumentation often used is the electron optical methods of LEED (Low Energy Electron Diffraction) and HEED (High Energy Electron Diffraction); electron microscopy, ellipsometry, internal reflection spectroscopy, thermonic and photoelectrid diodes.

It is the object of this thesis to develop a method of obtaining a clean, well ordered surface, and to incorporate into the LEED system a method for measuring surface work function change. The metal surface being studied is the (III) plane of copper. Similar work has been done by Farnsworth (1,2) on the (100) plane of copper.

CHAPTER II

THEORY

2.1.1 Low Energy Electron Diffraction

Prior to the development of electron optical techniques of LEED and HEED, precise and quantitative information about solid surface structures was not available. The electron optical techniques for studying surfaces give firm proof that many important properties of materials are largely determined by surface structure. These properties include electronic behaviour, corrosion, corrosion resistance and catalysis.

Many early theories on electronic behaviour of metals made the assumption that atoms on a surface plane had the same arrangement as the atoms in a parallel plane inside the crystal. Recent theories disprove this. The existence of a surface requires that the atoms in it have no neighbours on one side. The forces acting on them are therefore unsymmetrical, resulting in a modification of the atomic arrangement in the plane of the crystal face.

An even more significant effect is that real surfaces quickly become contaminated by adsorbed atoms. Where these atoms are adsorbed is strongly influenced by the position of the atoms on the clean surface.

The periodic arrangement of atoms in a crystal scatters material waves, producing diffraction patterns similar to those produced

by light scattering from a two dimensional system of line gratings. This phenomenon can be used to study surfaces. Provided the energy of the incident electrons is sufficiently low (~100 eV), only one or two atomic layers are penetrated. Hence the resulting diffraction pattern is representative of the crystal surface. Each crystal plane will have a characteristic diffraction pattern, since different atomic arrangement and spacing exists for different crystal planes.

A necessary condition that must be met for any diffraction effect to exist is that the incident electron waves must have wavelengths somewhat less than the largest grid spacing of the crystal surface. In general this spacing is of the order of a few angstroms.

X-rays and neutron waves have sufficiently short wavelengths, but because of their penetrating power they cannot be used to study the structure of the surface of a crystal. Electrons, however, make the ideal probe. Their wavelengths and energies can be adjusted so that they penetrate only the outermost atomic layers of a crystal surface and still cause a diffraction effect. Use of low energy electrons as a probe, then, gives a diffraction pattern of the crystal surface rather than the bulk. Thus the name Low Energy Electron Diffraction (LEED). An illustration of a Leed optical system is shown in figure 1.

If a metal is bombarded by a directed, monoenergetic electron beam, it will be observed that the secondary electrons emitted from the surface have a wide distribution of energy and angle with respect to the incident beam. A representative energy distribution is shown in

figure 2 (3). Only about one percent of all secondary electrons have the same voltage as the primary beam and these are incident electrons which have been elastically scattered. Since these elastically scattered electrons are the ones forming the diffraction pattern, the remainder of the electrons must be filtered out. This is done by means of a suppressor grid, set at a potential one percent lower than the potential of the incident electron beam.

The LEED system contains a fluorescent screen which will luminesce when electrons strike it with sufficient energy. Since the diffracted beams penetrate the suppressor grid with only a few electron volts, they have to be post-accelerated to give them sufficient energy to produce a fluorescent spot on the screen. This is accomplished by applying a potential of + 2kV to the fluorescent screen as shown in figure 1.

A shield grid is often added to provide a field free region between the crystal and suppressor grid so as not to distort the path of the slow moving electrons in this region.

The wavelength of the incident electron beam is given by

$$\lambda_e = \sqrt{\frac{150}{V}} \text{ Angstroms} \qquad (2.1.1)$$

where λ_e = electron wavelength [$\mathring{A}$]

V = electron accelerating potential [Volts]

2.1.2 Crystal Planes

Crystals can usually be classified with regard to atomic structure in terms of one of fourteen Bravais crystal lattices (4). One of the simplest of these, and the one of interest in this thesis, is the face centered cubic lattice. The arrangement illustrated below is a face centered cubic lattice (5).

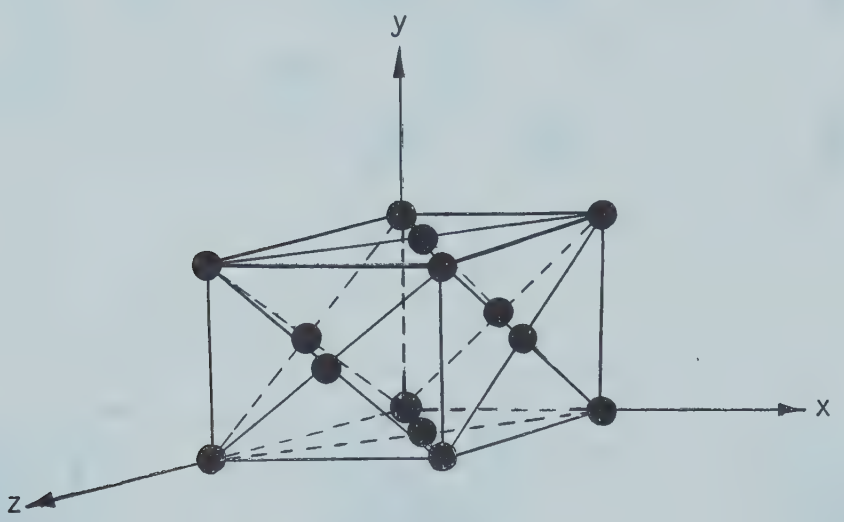

A two dimensional crystal plane is specified according to the way in which it intersects a three dimensional set of axis by Miller indices (hkl). These points are the inverse of the intersection points of the crystal plane with an arbitrary set of axis, xyz respectively. Each of these surfaces is made up of a repeating pattern of atoms that extends infinitely in two dimensions. These repeating patterns are usually specified in terms of the smallest repeating array of atoms defining the entire surface, called a unit mesh. The three most densely packed planes of a face centered cubic crystal and their corresponding

unit mesh are shown below:

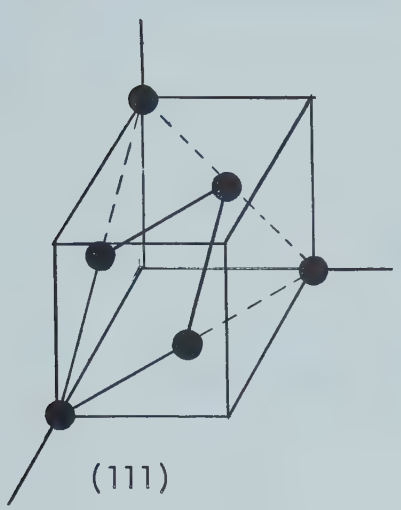

(111)

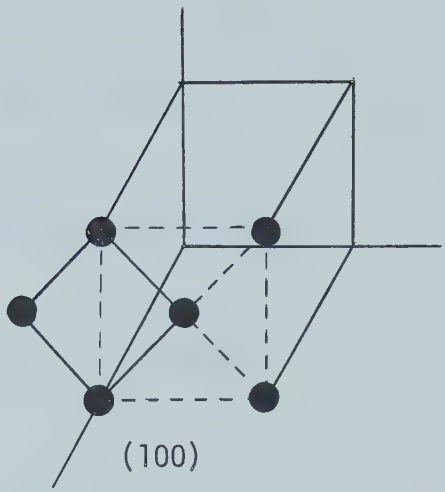

(100)

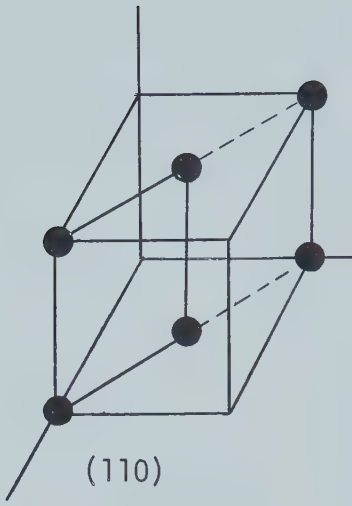

(110)

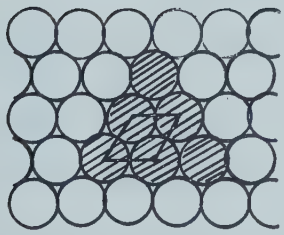

(111)

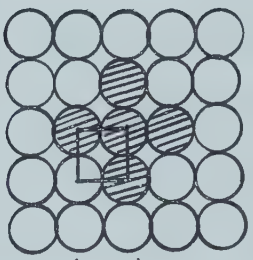

(100)

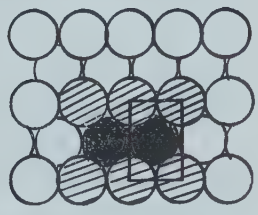

(110)

2.1.3 Line Gratings

An easy understanding of the diffraction pattern caused by a surface plane can be obtained by considering the interference effect of a simple line grating illustrated in figure 3. The condition for constructive interference of two diffracted wavelets is (6):

$$BC = n\lambda \quad n = 1,2,3 \ldots \tag{2.1.2}$$

From geometry

$$BC = AB\sin\theta \tag{2.1.3}$$

$$AB = d = \text{grid spacing}.$$

Relationship (2.1.2) then becomes

$$d \sin \theta = n\lambda \tag{2.1.4}$$

The constructive interference of wavelets appear as bright areas on the screen, whereas destructive interference ($n = \frac{1}{2}, \frac{3}{2}, \frac{5}{2} \ldots$) appear dark. The reflected beam (corresponding to constructive interference orders $n = 1,2,3 \ldots$) move (as the order n is increased) in a plane perpendicular to the line grating. As shown in figure 3, the diffracted orders (0,0), (1,0), (2,0) ... (n,0) are all in a line passing through the centre of the incident electron beam and perpendicular to the line grating.

In the LEED system, the crystal acts as a reflection grating instead of a transmission grating. No lens is necessary. The spots are images of the collimated beam. Lens 1 and the source are replaced by an electrostatically focused electron beam.

The optical system equivalent to our LEED system is a system having the light source in the focal plane of a lens, whereby projecting an image of the source on a screen. In between the lens and the screen, a collimated beam of small diameter is formed. This beam impinges on the crystal surface. Since any diffraction order is only an image of the source, shifting the line grating does not change the position of the diffraction order.

2.1.4 LEED Diffraction Patterns

LEED diffraction patterns are formed by constructive interference of electron waves elastically scattered from the two dimensional array of atoms in a crystal surface.

In analyzing such scattering it is convenient to regard the crystal as built up of (III) planes of atoms parallel to the principal facets and picture only electrons scattered from the outermost atomic plane. Establish a system of Cartesian coordinates as shown below, with Z direction perpendicular to the crystal surface.

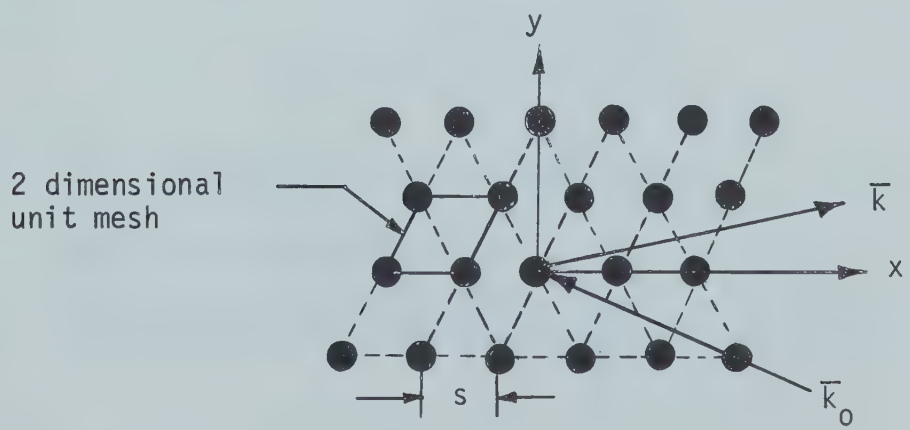

$\bar{k}_o$ = incident electron beam

$\bar{k}$ = scattered electron beam

S = least distance between atoms in a (III) plane

$= \frac{a}{2}\sqrt{2}$

$|\bar{k}| = 1/\lambda$

$\bar{k}$ = wave vector

Define an electron beam ($\bar{k}_o$), incident on the (III) plane, along the wave vector $\bar{k}_o$, whose direction cosines are ℓ_1, m_1, n_1. We observe the waves scattered in the direction $\bar{k}$ whose direction cosines are ℓ_2, m_2, n_2. For the scattered waves to interfere constructively, scattering must be in the $\bar{k}$ direction whose direction cosines are given by (7):

$$\ell_2 = \ell_1 + (p+r)\frac{\lambda}{s}$$

$$m_2 = m_1 + (p-r)\frac{\lambda}{\sqrt{3}S} \qquad (2.1.5)$$

$$n_2 = \pm (1-\ell_2^2-m_2^2)^{1/2}$$

where λ = wavelength of the incident light

p & r are any integers.

If $\bar{K}_o$ is at normal incidence, then $\ell_1 = m_1 = 0$, $n_1 = -1$

and

$$\ell_2 = (p+r)\frac{\lambda}{S}$$

$$m_2 = (p-r)\frac{\lambda}{S\sqrt{3}} \qquad (2.1.6)$$

$$n_2 = \pm (1-\ell_2^2-m_2^2)^{1/2}$$

Consider the most general case of an electron beam incident upon a line grating set at some arbitrary angle δ from the y axis.

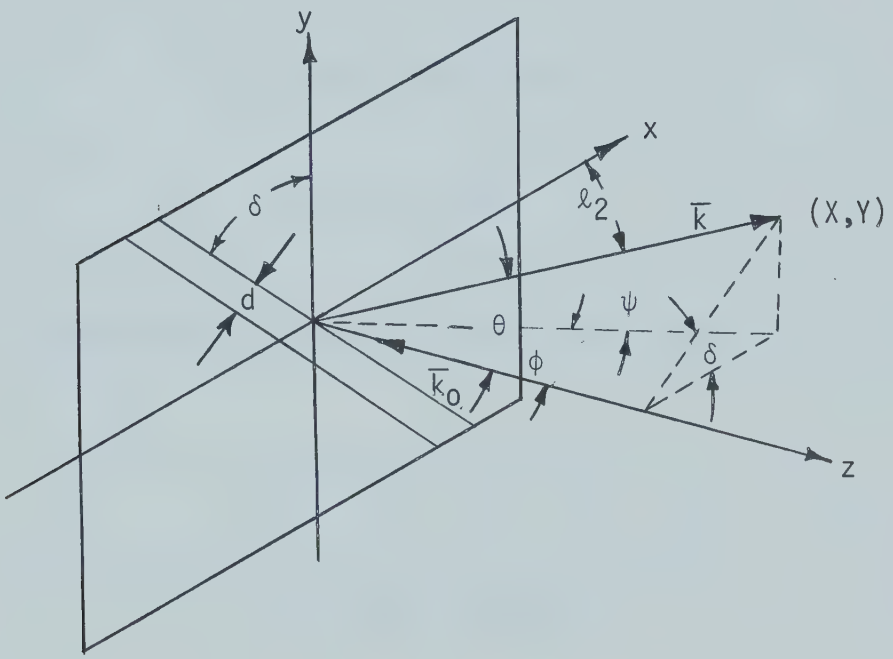

Equations (2.1.6) become:

$$\ell_2 = \cos\psi\sin\phi = (p+r)\frac{\lambda}{S}$$

$$m_2 = \sin\psi = (p-r)\frac{\lambda}{S\sqrt{3}} \qquad (2.1.7)$$

$$n_2 = \cos\theta$$

Further geometric relationships are given by the following equations:

$$\sin\psi = \sin\theta\sin\delta$$

$$\sin\phi = \sin\theta\cos\delta/\cos\psi$$

$$d = s\cos\delta \quad \text{for } \delta = 30$$

$$\cos\delta = \sqrt{3}\sin\delta$$

Equations (2.1.7) with the above relationships become:

$$\ell_2 = \sin\theta = (p+r)\frac{\lambda}{d}$$

$$m_2 = \sin\theta = (p-r)\frac{\lambda}{d} \qquad (2.1.8)$$

The above formulae give the angle at which constructive interference will occur. In order to predict the position of the spot expected on the LEED screen, it is necessary to correct for the viewing surface being a plane surface rather than a hemispherical surface.

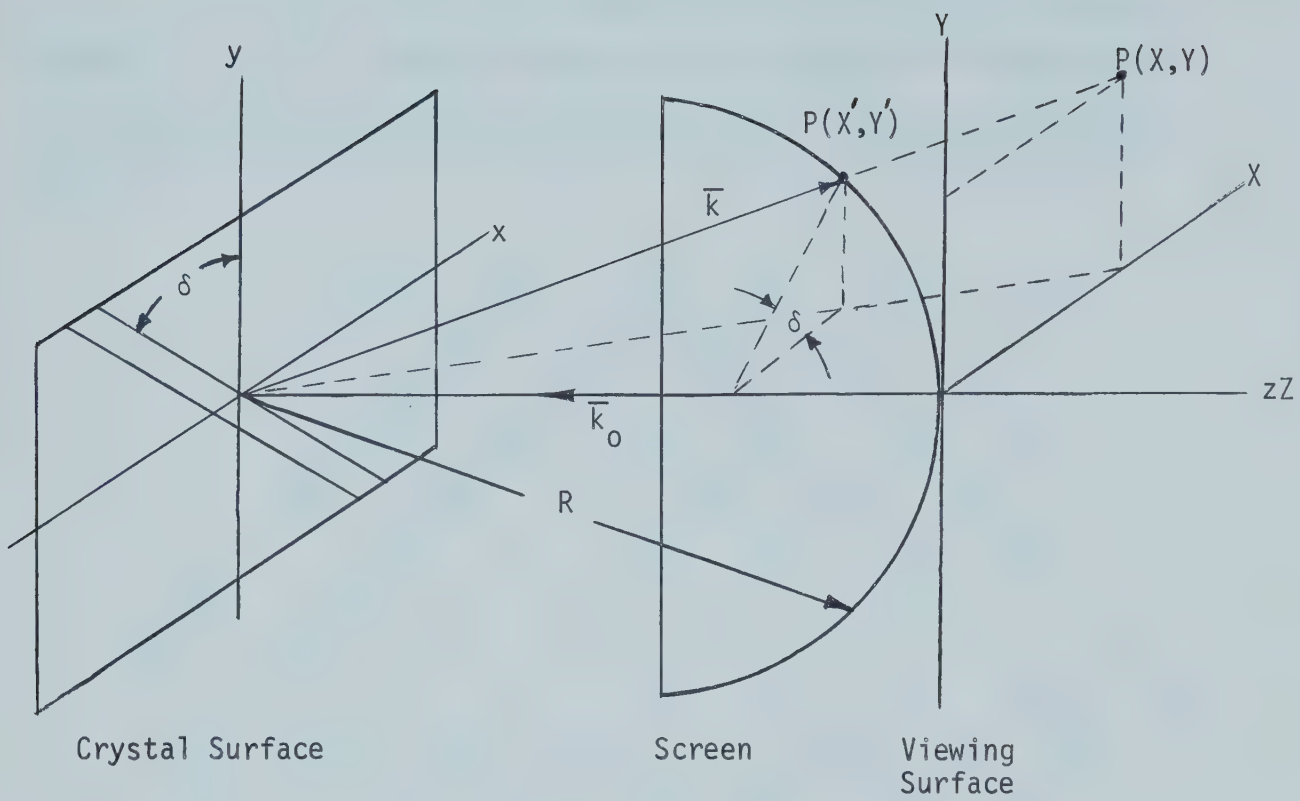

The geometric relationships that exist are:

$$X' = R \sin\theta \cos\delta$$

$$Y' = R \sin\theta \sin\delta \qquad (2.1.9)$$

where θ and δ are as previously defined

R = radius of screen.

For the (III) face of copper the minimum distance between atoms, S = 2.57Å . The diffraction pattern results from constructive interference from all parallel rows defined in the following diagram:

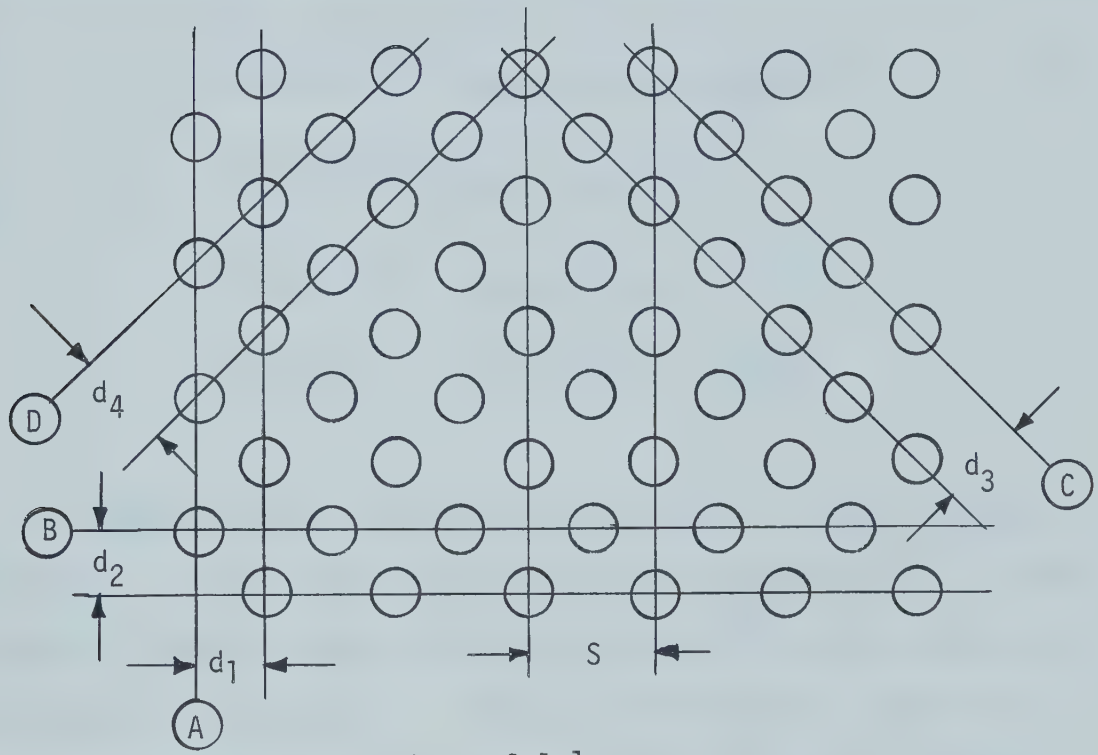

Figure 2.1.1

$$d_1 = \frac{S}{2} = 1.28 \text{ Å}$$

$$d_2 = d_3 = d_4 = 2.22 \text{ Å} \qquad (2.1.10)$$

$$d_5 = d_6 \ldots dn < 1.28 \text{ Å}$$

A large number of parallel rows of atoms could be chosen. Those with the largest grid spacing, d, are drawn.

Using formulae (2.1.9) and results (2.1.10), the position of diffraction spots produced by the parallel rows of atoms (A,B,C,D of figure 2.1.1) can be specified by coordinates X',Y'. For an incident electron beam voltage of 80 volts (λ = 1.37Å) the coordinates are:

$$A = A(X',Y') = \text{does not exist } (\frac{\lambda}{d} > 1)$$

$$B = B(X',Y') = B(0, \pm 0.613R)$$

$$C = C(X',Y') = C(\pm 0.532R, \pm 0.305R)$$

$$D = D(X',Y') = D(\pm 0.532R, \pm 0.305R)$$

Since the atomic rows of spacing d_1 and all others of smaller spacing (d_5 ... dn), do not satisfy the required condition ($\frac{\lambda}{d} > 1$), the only parallel rows of atoms contributing to the diffraction pattern are rows B,C,and D of figure 2.1.1. The type of diffraction pattern expected for an energy of 80 eV incident on the (III) face of a copper crystal is shown below.

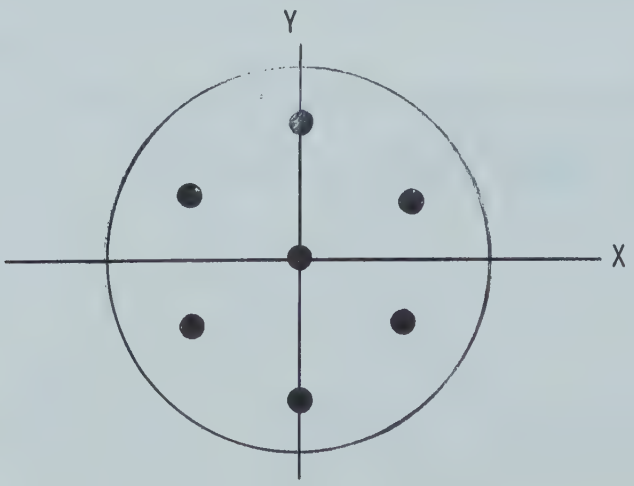

2.2.1 Electrons in Metals

For the purpose of discussing electronic behaviour in metals it is desirable to set up the potential-energy field for the three-dimensional spacial array of atoms that exists in the interior of a metal. The resultant potential energy at any point in the metal is simply the sum of the potential due to all the surrounding lattice ions.

The potential energy diagram resulting from two adjacent nuceli, (α,β) in a metal is shown below (8).

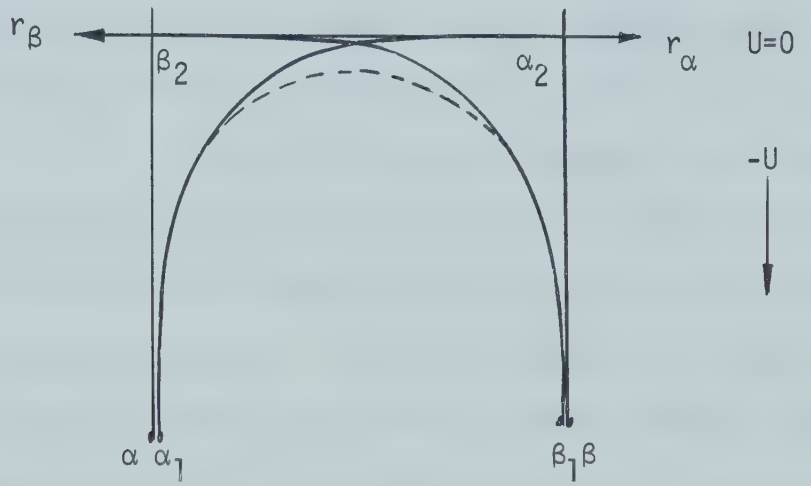

If the only two nuceli present were α and β, then the resulting potential energy diagram would be the sum of the two as shown by the dotted line α_1, β_1.

If however, instead of two nuclei, there were several parallel rows of nuclei α,β,γ,δ ..., the potential energy diagram would be as shown in figure 2.2.1.

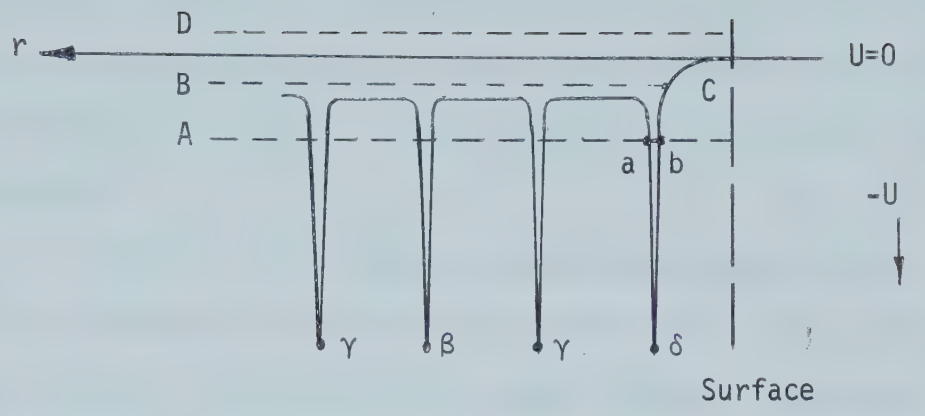

Figure 2.2.1

Classical electrostatics, which does not take the atomic structure into account, predicts the interior of a metal as an equipotential region. This, according to the above diagram is not true in the immediate neightbourhood of the nuclei, but as indicated by the flat portion, the potential energy is approximately constant for the greatest portion of the metal in the volume between the nuceli.

An electron in a metal with potential energy corresponding to level A in figure 2.2.1 will collide with and rebound from the potential wall at ab. Its motion is almost restricted to the region ab and cannot drift very far from the nucleus. It is fittingly called a bound electron.

When speaking of conduction in a metal we are interested in the free electrons. Such an electron is one having energy corresponding to (BC) in the diagram. Since at no point in the metal is the total energy converted to potential energy, at no point is the velocity zero. The electrons then travel more or less freely through the metal. However

when an electron reaches the surface it collides with a potential barrier resulting from the surface charge distribution. At this point its kinetic energy is reduced to zero, and the electron returns back into the metal.

An electron having energy corresponding to point D of figure 2.2.1, does not collide with a potential wall, and is able to leave the surface. It is these high energy electrons that are of interest in thermonic emission.

Fermi-Dirac statistics predicts the probability of an electron having an energy E to be:

$$F(E) = \frac{1}{e^{(E-E_F)/KT} + 1} \qquad (2.2.1)$$

K = Boltzman's constant

T = temperature of the metal

E_F = Fermi Energy

= Highest occupied energy level at T = ÔK

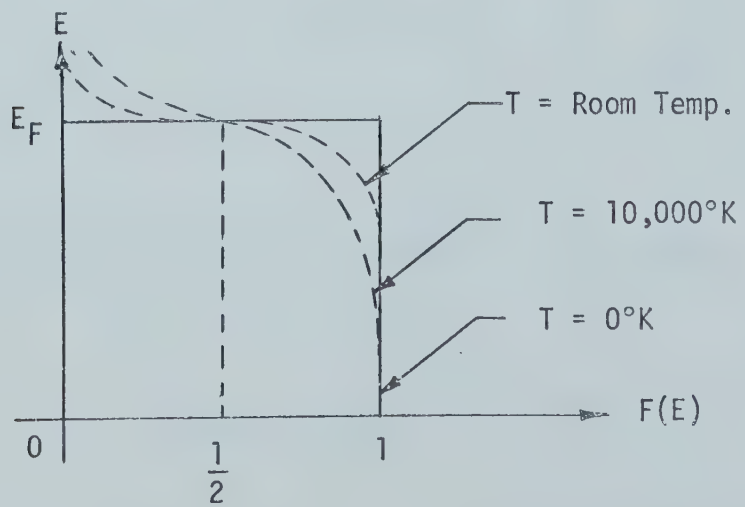

From the preceding figure it can be seen that at $T = {}^{o}OK$ no electrons exist with energies greater than the Fermi Energy E_F. As the temperature of the metal is increased, $(T > {}^{o}OK)$ there is a certain probability that electrons exist with $E > E_F$. Even at very high temperature the number of electrons in these high energy states is a very small percentage of the total number of electrons.

2.2.2 The Concept of Work Functions

In order for one of these high energy electrons to escape the metal surface, it must possess an amount of energy greater than that represented by the height of the surface potential barrier. Figure (2.2.1) is redrawn in figure (2.2.2) with all potential variations within the metal being omitted except the potential barrier at the surface.

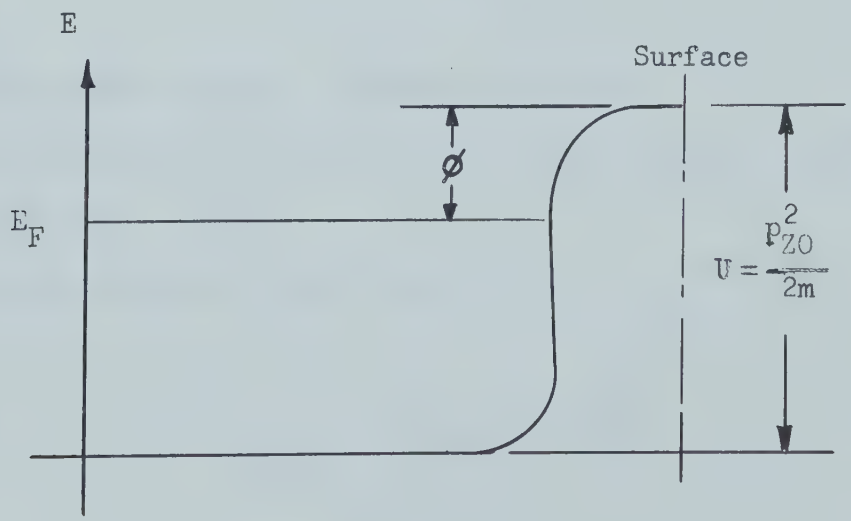

Figure 2.2.2

If the momentum state corresponding to the top of the potential barrier is p_{zo}, only those electrons with momenta $p_z > p_{zo}$ will escape. There is, however, a certain probability that even some of the electrons with $p_z > p_{zo}$ will be reflected at the surface. This can be represented by a reflection coefficient, r, such that the fraction (1-r) of the electrons with sufficient z momentum are able to escape.

The number of electrons leaving on emitter surface per unit area, per unit time is $n(p_z)\, dp_z\, V_z$ where $n(p_z)dp_z$ is the number of electrons per unit volume with momentum p_z in the interval dp_z and V_z is the z component of the electron velocity. The emission current is (9):

$$I = \int_{p_{zo}}^{\infty} V_z(1-r)\, n(p_z)\, dp_z \qquad (2.2.2)$$

The number $n(p_z)dp_z$ if found as follows:

The energy distribution for electrons in a metal is given by equation 2.2.1.

Using the perfect gas assumption:

$$E = E_{kinetic} = \frac{p_x^2 + p_y^2 + p_z^2}{2m} \qquad (2.2.3)$$

Using 2.2.3 equation 2.2.1 becomes:

$$F(E) = F(p_x,p_y,p_z) = \frac{1}{e^{\frac{p_x^2+p_y^2}{2mKT} - \frac{E_F}{KT}} \cdot e^{\frac{p_z^2}{2mKT}} + 1} \qquad (2.2.4)$$

$F(p_x,p_y,p_z) \cdot Z(z) =$ Average number of electrons with momenta p_x,p_y,p_z, in the momentum volume element dp_x, dp_y, dp_z .

$$= N(p_x,p_y,p_z)dp_x dp_y dp_z \qquad (2.2.5)$$

From quantum mechanics the number of allowed states in momentum space $dp_x\ dp_y\ dp_z$ is:

$$Z(x,y,z) = Z(z) = V\frac{dp_x\ dp_y\ dp_z}{h^3} \qquad (2.2.6)$$

where V = volume of metal

h = Planck's constant

The Pauli Exclusion principal allows two electrons (with opposite spin) per quantum state giving:

$$Z(z) = 2V\ \frac{dp_x\ dp_y\ dp_z}{h^3} \qquad (2.2.7)$$

With relationship 2.2.7, equation 2.2.5 becomes:

$$\frac{2V}{h^3} F(p_x,p_y,p_z)\, dp_x\, dp_y\, dp_z = N(p_x,p_y,p_z)\, dp_x\, dp_y\, dp_z) \quad (2.2.8)$$

Integrating 2.2.8 over $dp_x\, dp_y$ and substituting $N(p_x,p_y,p_z) = n(p_x,p_y,p_z)V$, equation 2.2.8 becomes:

$$n(p_z)\, dp_z = \frac{2}{h^3} dp_z \int_{-\infty}^{+\infty}\int_{-\infty}^{+\infty} \frac{dp_x\, dp_y}{e^{(E_z-E_F)/KT} \cdot e^{\frac{p_x^2+p_y^2}{2mKT}} + 1} \quad (2.2.9)$$

Cylindrical polar coordinates are introduced to facilitate integration.

$$p_x = p_r \cos\theta$$
$$p_y = p_r \sin\theta \quad (2.2.10)$$

Remembering that $|E_z-E_F| > \phi >> kT$ for an electron to escape, equation 2.2. can be integrated to give

$$n(p_z)\, dp_z = \frac{4\pi KT}{h^3}\, e^{E_F/KT} \cdot e^{-p_z^2/2mKT} \quad (2.2.11)$$

The emission equation, equation 2.2.2 then becomes

$$I = A(1-r)\, T^2\, e^{(\frac{E}{KT} - \frac{p_{zo}^2}{2mKT})} \quad (2.2.12)$$

where $A = \frac{4\pi meK^2}{h^3}$.

From figure (2.2.2) it follows that

$$\phi = \frac{p_{zo}^2}{2m} - E_F \qquad (2.2.13)$$

ϕ = work function of the metal.

Using relationship (2.2.13) equation (2.2.12) becomes the Richardson equation,

$$I = A(1-r)\, T^2 e^{-\phi/KT} \qquad (2.2.14)$$

2.2.3 Displacement Diode Characteristics

One of the best known methods for investigating surface work functions is the thermonic diode method. For a diode with anode and cathode work functions of ϕ_a and ϕ_c respectively, the potential barrier that must be overcome by electrons leaving the cathode to reach the anode is $\phi_a - \phi_c = \Delta\phi$. Schematically this situation is represented below.

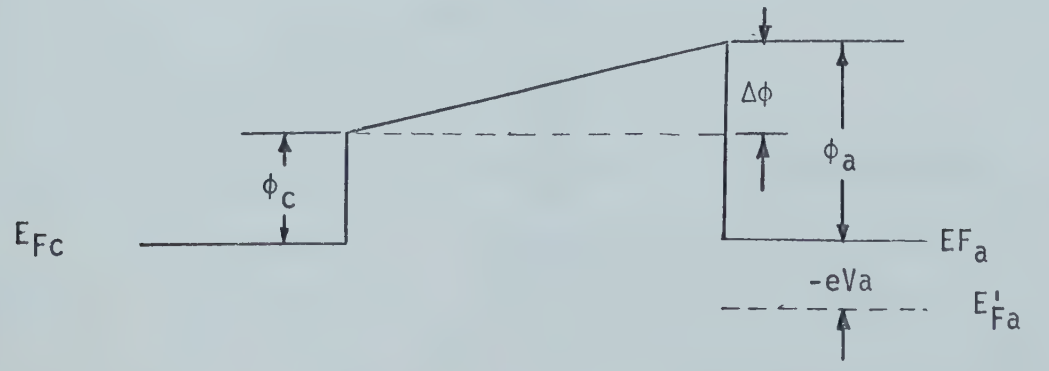

Electrons must have sufficient energy to at least reach the anode, if current is to flow through the diode. That is energy of

$$+ \phi_c + \Delta_\phi = \phi_a \qquad (2.2.15)$$

Hence the equation for the diode current is:

$$I = A(1-r)T^2 e^{-\phi_a/KT} \qquad (2.2.16)$$

T = temperature of cathode.

Thermonic diode characteristics are usually obtained by applying a bias voltage ($-eV_a$) to the anode. The result being an increase or decrease in the anode Fermi level. A typical diode characteristic is shown in figure (2.2.3).

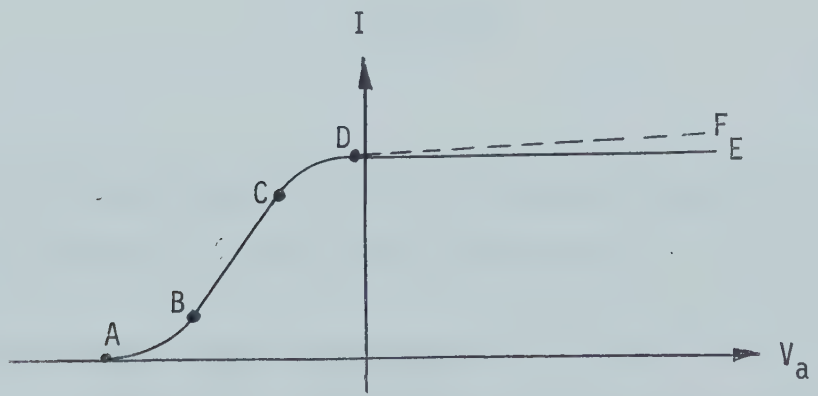

Figure 2.2.3

When the anode bias is greater than $\Delta\phi$ all electrons emitted at the cathode are collected at the anode, and diode current is a constant depending on ϕ_c (DE in figure 2.2.3). In the region (DE) a slight increase in current is observed with increased anode voltages (DF). This increase is due to the reduction of the emitter work function due to the external accelerating field (10).

In the region (CD), the electrons reaching the anode are very low velocity and are partially repelled by retarding field, causing an electron cloud to form at the emitter. This electron cloud, acting as a space charge tends to increase the emitter work function thus reducing diode current.

For the retarding field region (BC), the current collected at the anode is less than that emitted by the cathode due to the increased potential barrier ($-eV_a$) that must be overcome. The equation for the diode current in this region is

$$I = A(1-r)T^2 e^{-(\phi_a - V_a)/KT} \qquad (2.2.17)$$

It is this region that is useful in determining ϕ_a since the effect of external fields on diode current are minimal.

2.2.4 Adsorption Effect on Work Functions

The work function of a metal is greatly influenced by the presence of an external electric field. Depending on the sign (accelerating or decelerating) of the field, the work function is lowered

or raised.

A similar effect is observed due to any modification of the charge distribution on the metal surface. Adsorption processes change the surface charge distribution, hence changing the surface work function. Consider the work function change involved in two of the simplest forms of adsorption, illustrated in figure 2.2.4.

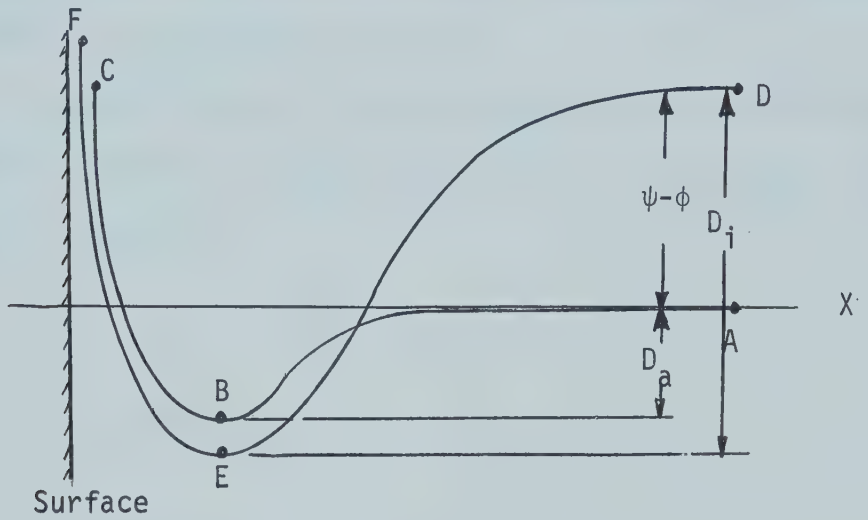

Figure 2.2.4

An atom approaching a metal surface is subject to a Van der Waals force field resulting in a potential energy curve of the form ABC of figure 2.2.4. If the atom is ionized at point A and the electron goes to the metal, the potential of the original atom at A is increased by an amount $\psi-\phi$ where ψ is the ionization energy of the atom and ϕ is the work function of the metal. The resulting ion is subject to an attractive image potential given by DEF of figure 2.4. If $|D_i-(\psi-\phi)| < |D_a|$ the atom is adsorbed as an ion, since the most stable state is the state of lowest free energy. The effect of adsorption of ions on

work function is a decrease for positive ions, and an increase for negative ions.

If $|D_i-(\psi-\phi)|>|D_a|$ the atom will be adsorbed as a neutral at B. In this case dipoles, resulting from polarization by the surface charge distribution of the metal, are adsorbed. The net result is an increase of the work function when the positive pole of the adsorbed dipole points away from the surface, and a reduction of the work function for an inward pointing dipole.

It should be noted that the surface charge distribution is different for different crystal faces resulting in different work functions for each face.

CHAPTER III

EXPERIMENTAL APPARATUS

3.1 Vacuum System

The arrangement of the vacuum system including the LEED system is shown in figure 4.

All components in the ultrahigh vacuum region were constructed of either glass or stainless steel, all joints were welded using argon inert gas technique, and shop constructed parts were cleaned as outlined in Appendix I.

Varian conflat flanges fitted with OFHC copper gaskets were used for all demountable joints.

The system was outgassed by baking at 300°C in a temperature regulated Marinite oven for a period of 8 hours.

3.2 Pumps

During bakeout the system was pumped by means of a 100 ℓ/sec diffusion pump fitted with a liquid nitrogen cold trap.

After bakeout, the diffusion pump was valved off and the system was then pumped with a 15 ℓ/sec diode ion pump. An ultimate pressure of about 5×10^{-10} torr was achieved.

3.3 Pressure Gauges

A partial pressure gauge, capable of measuring partial pressures

as low as 10^{-10} torr was used to measure pressures. In addition to determining total pressure, the partial pressure gauge has the advantage of giving additional information on residual gas in the system, and is used as a monitor for partial pressures of gases present during experiments. It also serves as a sensitive leak detector.

Pressure during bakeout and initial roughing was monitored by a thermocouple gauge and a cold cathode ionization gauge incorporated into the pump stand.

3.4 Gas Inlet

Gas admittance into the system was accomplished with a bakeable, variable leak valve having a minimum leak rate of 1×10^{-11} ℓ/sec. A liquid nitrogen cold trap was fitted to the line ahead of the leak valve.

The LEED system used was the Veeco model LM-1000. A discussion of individual components follows below.

3.5.1 Crystal Manipulator

The crystal manipulator was capable of swinging the crystal across the path of the electron gun and into position for cleaning and work function measurement, but did not allow tilting or rotation.

3.5.2 Electron Gun Optics

The electron gun produced an electrostatically focused electron beam with energies ranging from 0-300 eV corresponding to wavelengths from 0.5Å to 18Å. An indirectly heated oxide coated

cathode was used to reduce filament glare in the diffraction pattern.

3.5.3 Specimen Cleaning Facility

Provision was made in the Veeco LM-1000 for electron bombardment heating of the target crystal in order to evaporate surface contaminants.

3.6 Work Function Measurement

The circuit for retarding field diode measurement shown in figure 5 was incorporated into the electron bombardment cleaning circuit installed in the LM-1000 equipment. While measuring work function changes, voltages were measured with a digital voltmeter, and currents were monitored with a sensitive electrometer. Additional regulated voltages were used to provide the retarding potential and constant voltage input to the filament. The tungsten filament used for specimen cleaning in the LEED chamber served as the cathode of the retarding field diode.

3.7 Crystal Holder

Crystals were suspended between two strips of molybdenum, clamped to the LEED crystal mount.

3.8 Temperature Measurement

Crystal temperatures during cleaning were measured with a radiation thermometer. An emissivity of copper of 0.06 (10) was used. Temperatures measured with the radiation thermometer were thought to be accurate within $\pm$ 50°F.

CHAPTER IV

EXPERIMENTAL RESULTS AND DISCUSSION

4.1 Sample Preparations

A single copper crystal crystal one centimeter square and fifteen centimeters long was prepared from copper stock by multiple passes on a zone melting induction furnace. The final purity of the clean end of the crystal was about 99.99% pure.

Two samples one centimeter square and 0.060 centimeters thick were cut from the copper bar with a 0.008 inch diameter wire saw and boron carbide abrasive, after orientating the required face by X-ray diffraction. The samples were then polished (5μ diamond paste) and lightly etched with a solution of 70% nitric acid and 30% acetic acid. The surface roughness of the prepared specimen was 5 to 20 micro inches, centre line average (see Appendix II for explanation of centre line average). Microscope pictures of the surface are shown in figures 6 and 7. Prior to mounting the specimen in the LEED system, the orientation of the desired crystal plane was specified to within 1 degree. The X-ray diffraction picture and analysis (4,11) is presented in figures 8 and 9.

4.2 Specimen Cleaning

Following mounting of the sample in the LEED system, and system bakeout, samples were degassed for about 200 hours at temper-

atures ranging from 1000°F initially, to 1200°F for the final 24 hours. During this time observations were made for diffraction patterns and work functions were measured.

Curve A of figure 11 is the retarding potential curve obtained following this initial 200 hours of degassing of crystal 1. A diffraction pattern was not visible following this surface treatment.

Crystal 1 was then heated for 15 minutes in an atmosphere of 4×10^{-6} torr hydrogen, followed by a 4 hour anneal of 1200°F with a system pressure of 3×10^{-9} torr. The retarding potential after this treatment did not change from that of the original surface. A diffraction pattern was still not visible.

An additional 4 hours of heating crystal 1 at 1200°F in a hydrogen atmosphere of 4×10^{-6} torr followed by a 24 hours anneal at 1500°F did not clean the surface enough to produce a diffraction pattern. The retarding potential data is given by curve B of figure 11.

Another 8 hours of heating crystal 1 at 1200°F in 4×10^{-6} torr hydrogen, followed by a 24 hour anneal at temperatures of 1500-1600°F, produced the diffraction pattern expected for a clean, ordered (III) face, shown in figure 10. This final heat treatment evaporated an extensive amount of copper onto the LEED bell jar. As a consequence, the photograph of figure 10 is somewhat blurred. Subsequent temperature measurements were also in error due to the copper film on the LEED viewing port.

The retarding potential data obtained after the first diffraction pattern was observed is given by curve C of figure 11. The work function of crystal 1, from the retarding potential data of figure 11, was increased by 0.55 =eV by the hydrogen reduction - annealing, surface treatment.

It was not evident from the tests performed on crystal 1 if hydrogen reduction contributed to the cleaning process. Further tests on crystal 1 were not possible due to its destruction by melting during further heat treatment.

A second series of tests were performed on crystal 2, consisting of only the heat treatment used on crystal 1. Curves D, E and F of figure 11 were obtained after annealing for identical times and temperatures as crystal 1. The presence of a clean well ordered surface was not verified by LEED due to the destruction of the cathode when crystals were changed. The work function, according to figure 11, of the surface of crystal 2 after heat treatment was observed to be increased by 0.55 eV.

These results indicate that the clean surface obtained with crystal 1 could have been obtained with the high temperature heat treatment alone.

The difference in the diode currents for crystal 1 and 2 resulted from changing the voltmeter for measuring V_a.

The destruction of crystal 1 prevented any tests to determine the length of time required for the surface to become contaminated and the length of high temperature (1500-1600°F) heat treatment required to

reclean the surface.

Mass analysis of residual gas during hydrogen reduction indicated the reducing atmosphere to be 99.92% hydrogen, .01% H_2O, .02% N_2 and .05% Ar. Partial pressures of residual gases at the end of the 24 hour anneal at 1500-1600°F were below 2×10^{-10} torr.

4.3 Adsorption of Gases

The clean (III) face of copper was exposed to quantities of hydrogen, nitrogen and oxygen at temperatures of approximately 500°F. The dosages were measured by taking the time integral of the true partial pressure read from the partial pressure gauge. Assuming a sticking probability of one and test gas at room temperature, exposures of 1.02×10^{-6} torr-sec, 3.3×10^{-6} torr-sec. and 3.65×10^{-6} torr-sec were sufficient to produce a monolayer coverage of hydrogen, nitrogen and oxygen respectively on the crystal surface.

All gas exposures were made with the partial pressure gauge filament on and inlet gas passing through a liquid nitrogen cooled cold trap. The gauge magnet was removed during all tests except during hydrogen exposures where it was accidently left connected.

A clean well ordered surface prior to gas exposures was assured by annealing for 8 hours at 1500-1600°F. While the crystal was at this temperature, the electron bombardment beam power was approximately 0.8 watts. The crystal color at a temperature of 1500°F was bright orange.

All adsorption studies were performed on crystal 2.

During the work function measurements, the filament voltage

was set at 1.7 volts, and the grid voltage was + 40 volts. The emission current was calculated to be approximately 1×10^{-4} amps.

4.3.1 Hydrogen Exposure

A series of hydrogen exposures at pressures of 10^{-8} torr for periods of 1 - 60 minutes were performed at crystal temperatures of 500°F and 1500°F.

Curve A of figure 12 represents the retarding potential curve at 500°F before hydrogen exposure. Curve B was obtained following a hydrogen exposure of 6×10^{-5} torr-sec at a crystal temperature of approximately 500°F. Curve C was obtained following an additional hydrogen exposure of 3.6×10^{-4} torr-sec. at a crystal temperature of approximately 500°F.

The results of a second test with a hydrogen exposure of 1×10^{-4} torr-sec. and a crystal temperature of approximately 1500°F are presented in Table II, column D*.

At crystal temperatures of 500°F and 1500°F there was no observed work function change resulting from hydrogen exposure. It was assumed that hydrogen did not adsorb. This is in agreement with the results obtained by Farnsworth (2) for the (100) face of copper.

4.3.2 Nitrogen Exposure

Following hydrogen exposure the system was allowed to pump for 48 hours to remove any residual hydrogen from the previous experiment. The crystal was then cleaned for 8 hours at a temperature of

approximately 1500°F.

The retarding potential for the clean surface at 500°F is curve A of figure 13. Curves B and C were obtained after nitrogen exposures of 3×10^{-5} torr-sec. and 1.5×10^{-4} torr-sec. Retarding potential data obtained after a total nitrogen exposure of 1.8×10^{-3} torr-sec. is given in column D*, Table III. Following a 4 hour anneal at 1500-1600°F, the retarding potential data was the same as that of curve A.

According to curves B,C, and D, exposures of nitrogen did not change the surface work function. Farnsworth (2) found no change in work function or diffraction pattern when the 100 face of copper was exposed to nitrogen.

Tests were not performed at elevated temperatures because the method of heating the specimen produces some nitrogen ions which according to Farnsworth (3) do adsorb. Since there were no facilities incorporated in the work function measuring circuit for biasing the specimen to seperate the different ionic species of nitrogen, and the LEED system was not functional, any results obtained would have been meaningless.

4.3.3 Oxygen Exposures

Following the procedure used in section 4.3.2 for cleaning prior to nitrogen exposure, the retarding potential data for curve A of figure 14 was obtained. Curves B, C and D were obtained after oxygen exposures of 2×10^{-7} torr-sec., 3×10^{-6} torr-sec., and 3.8×10^{-5} torr sec. Recleaning for 4 hours produced the clean surface of

curve A.

Curve B represents an increase of the surface work function by 0.35 eV. Further oxygen exposures of 3×10^{-6} torr-sec. and 3.8×10^{-5} torr-sec. produced an increase of the surface work function of 0.6 eV.

It is not possible with the results from this experiment to predict the surface structure present following any of the oxygen exposures. It may be noted that LEE and Farnsworth (2) found a lowering of the surface work function of 0.4 eV on the (100) face of copper following an oxygen exposure of 2×10^{-3} torr-sec.

4.4 General

Photomicrographs under 200 magnification of the crystal surface prior to, and after 400 hours of high temperature (1500-1600°F) surface treatment are shown in figures 6 and 7.

The photomicrograph of figure 6 shows very little evidence of mechanical working due to polishing. The small black spots in both figures 6 and 7 are believed to be impurities either from polishing or from the copper single crystal from which the specimens were cut.

In figure 7 the bright areas are the remaining portions of the crystal that are approximately parallel to the original (III) face. The darker areas are craters formed by copper evaporation during the cleaning process. The striations present in figure 7 are believed to be a result of polishing. Their presence in figure 7 and

absence in figure 6 can be explained by considering the mechanisms involved in polishing. Polishing removes surface irregularities, but induces some sub surface irregularities. After evaporation of several layers of copper, these sub surface undulations will appear on the surface.

As a result of about 400 hours of heating the crystal at evaporation temperatures, approximately 70% of the original surface was destroyed by crater formation.

The retarding potential curves of the clean surface initially (50 hours of cleaning), prior to oxygen exposure (250 hours cleaning) and at the end of experiments (400 hours of cleaning) are replotted in figure 15. The surface work function change of the clean surface between the beginning of experiments and completion was - 0.40 eV. It was believed that this change resulted from destruction of the surface by crater formation and electrical current leakage caused by the extensive amounts of copper evaporated onto the diode.

The destruction of the surface was also a possible reason for the lack of intensity in the diffraction pattern.

4.5 Errors

Two types of experimental errors significant enough to influence results were present during these experiments.

4.5.1 Work Function Measurement

These errors arose as a combination of instrument noise, background noise, and changes in surface properties while retarding

potential data was being obtained. These errors were minimized by repetition of the experiments and readings. In general the reproducibility of a curve, over a period of twenty minutes was $\pm$ 0.05 eV.

4.5.2 Temperature Measurement

Before the evaporation of a copper film onto the viewing port of the LEED system, the radiation thermometer gave reproducible temperature readings of $\pm$ 20°F. The choice of emissivity of 0.060 gave temperature readings 200°F lower than the actual crystal temperature (Determined by melting the crystal).

After large amounts of copper evaporated onto the LEED bell jar, the radiation thermometer could no longer be used. Temperatures were determined by color and electron bombardment power. It was estimated that a temperature of 1500°F, which was used throughout the experiments, could be obtained to $\pm$ 150°F.

CHAPTER V

CONCLUSIONS

1. A clean (III) copper surface can be obtained by heating to evaporation temperatures (1500-1600°F) for 50 hours in a vacuum of 2×10^{-9} torr, after an initial 200 hours of degassing at 1000°F.

2. The high temperature heating process produces a clean surface but tends to create craters on the surface. Extended cleaning will destroy most of the surface.

3. Hydrogen did not aid in surface cleaning by reduction of copper oxides.

4. Hydrogen did not adsorb on the (III) copper surface at temperatures of 500°F and 1500°F.

5. Molecular nitrogen does not adsorb on a (III) copper surface at 500°F.

6. Oxygen does adsorb on the (III) face of copper. An oxygen exposure of 3.8×10^{-5} torr-sec. resulted in an increase of the surface work function by 0.60 electron volts.

BIBLIOGRAPHY

1. SCHLIER, R.E., and FARNSWORTH, H.F., "Low Energy Electron Diffraction Investigation of Chemisorbed Gases on the (100) Faces of Copper and Nickle Single Crystals", Journal of Applied Physics 25, No. 10, 1333 (1954).

2. LEE, R.N., and FARNSWORTH, H.F., "LEED Studies of Adsorption on Clean (100) Copper Surfaces", Surface Science 3, 461-479, (1965).

3. GERMER, L.H., "The Structure of Crystal Surfaces", Reprint, Scientific American, Vol. 212, No. 3, 32-41, (1965).

4. CULLITY, B.D., "Elements of X-ray Diffraction", Addison Wesley Metallurgy Series (1956).

5. MAY, J.W., "Electron Diffraction and Surface Chemistry", Reprint Industrial and Engineering Chemistry, 18-39, July (1965).

6. RESNICK, R., and HALLIDAY, D., "Physics for Students of Science and Engineering", John Wiley and Sons Publishing Company (1962).

7. DAVISSON, C.J., and GERMER, L.H., Diffraction of Electrons off a Nickel Crystal", Physics Review 30, 705, (1927).

8. MILLMAN, J., and SEELY, S.,"Electrons" McGraw-Hill Book Company Inc. (1941).

9. CARR, D.M., "Surface Work Functions", Unpublished.

10. HERRING, C. and NICHOLS, M.H., "Thermonic Emission" Review of Modern Physics", Vol. 21, 185 (1949).

11. WOOD, E.A., "Crystal Orientation Manual" (1965). Bell Telephone Laboratories, Inc., Columbia University Press (1963).

12. LANDER, J.J., "Low-Energy Electron Diffraction and Surface Structural Chemistry", Progress in Solid State Chemistry, Vol. 2, 26-116, (1965).

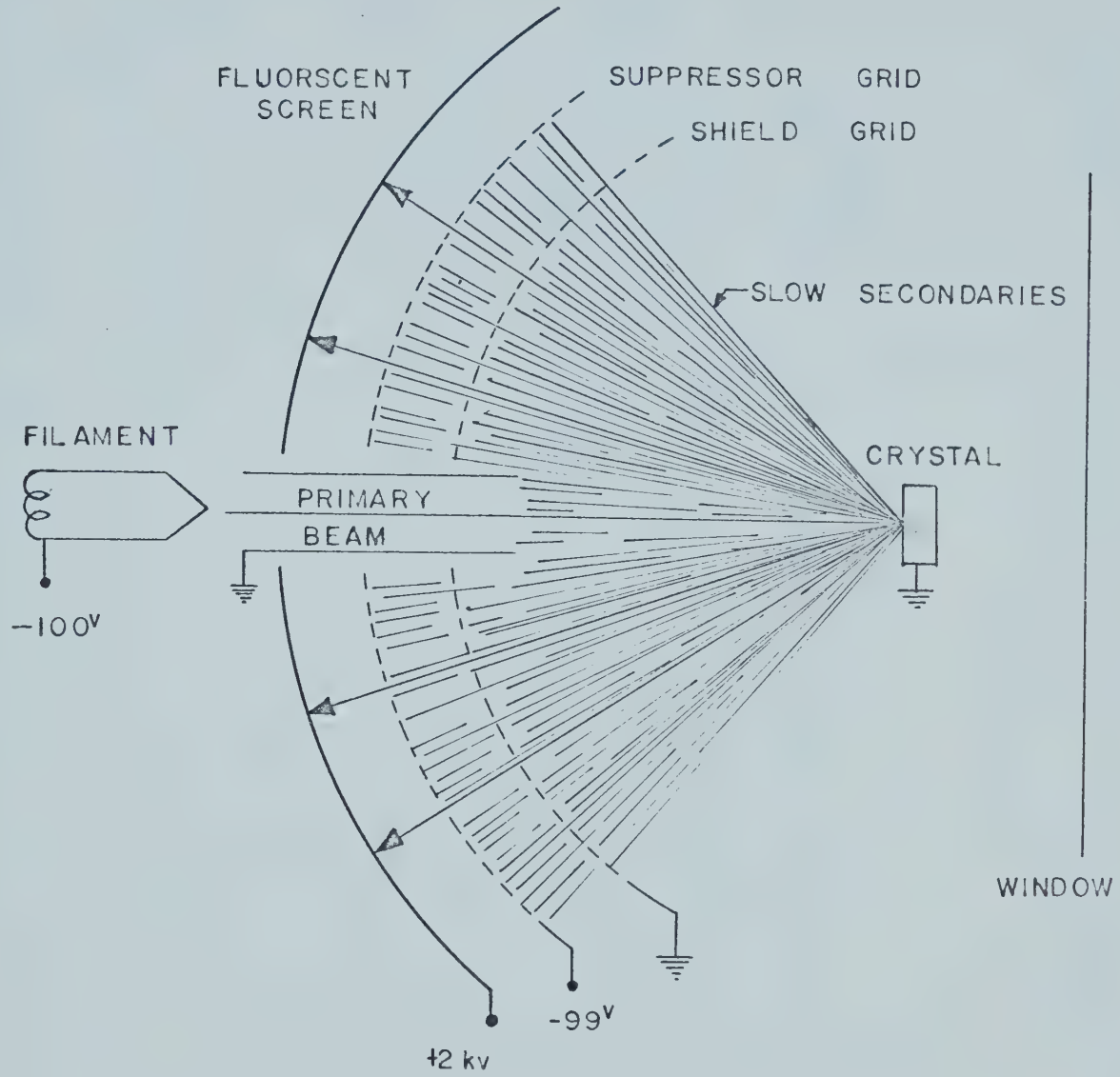

— FIGURE 1 —

LEED OPTICS (12)

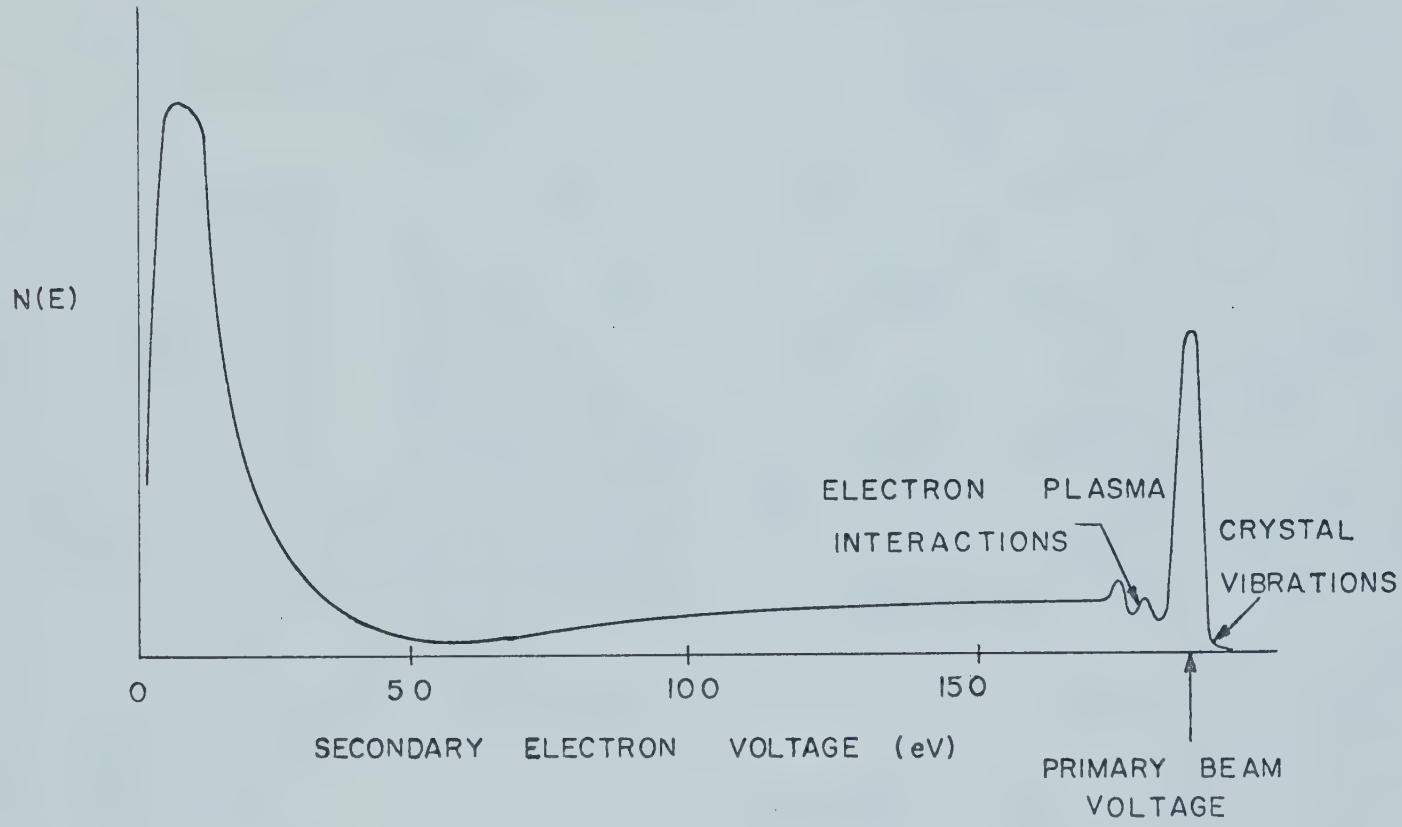

— FIGURE 2 —

ENERGY SPECTRUM OF SECONDARY ELECTRONS(3)

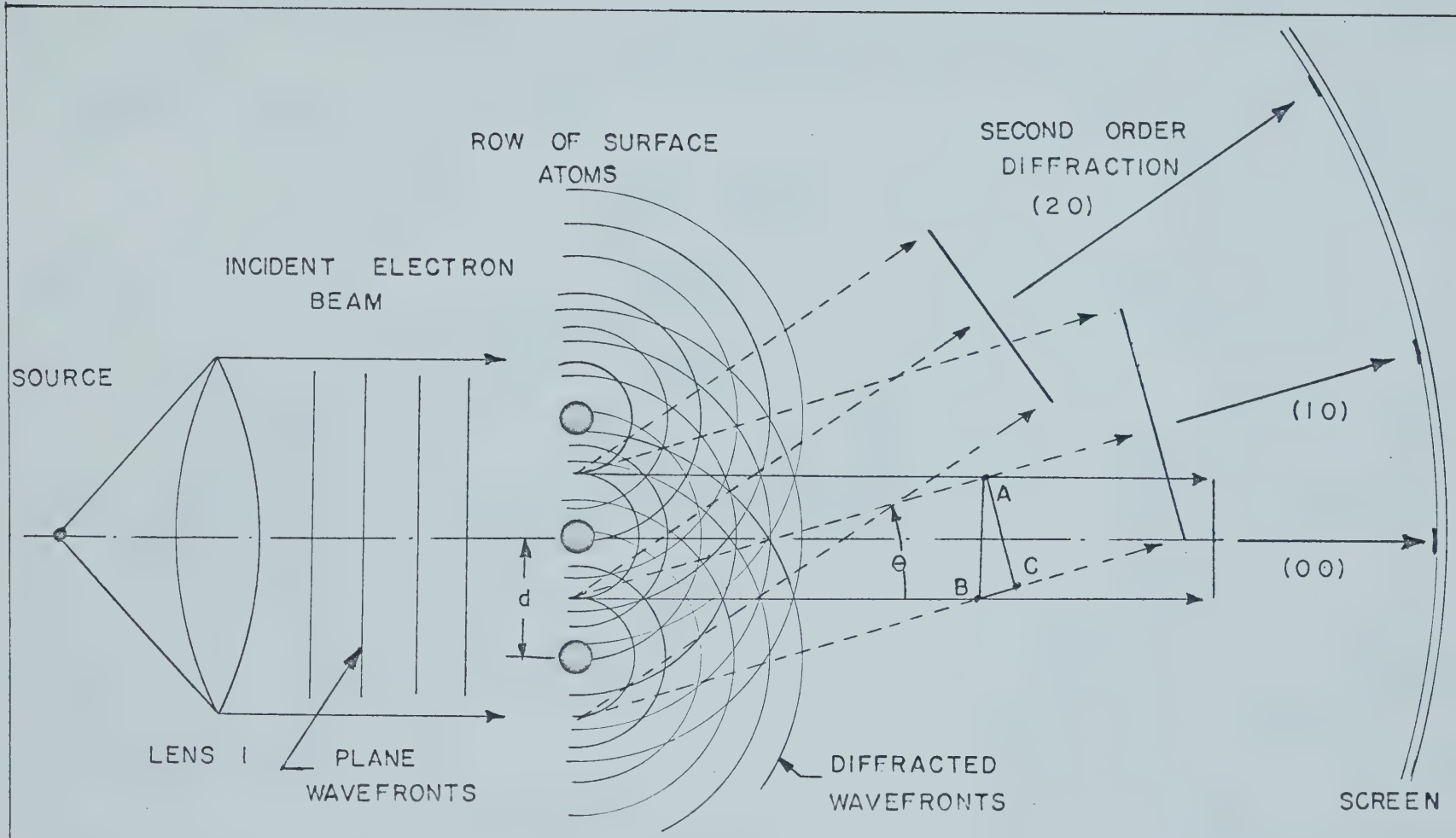

— FIGURE 3 —

OPTICAL LINE GRATING SYSTEM

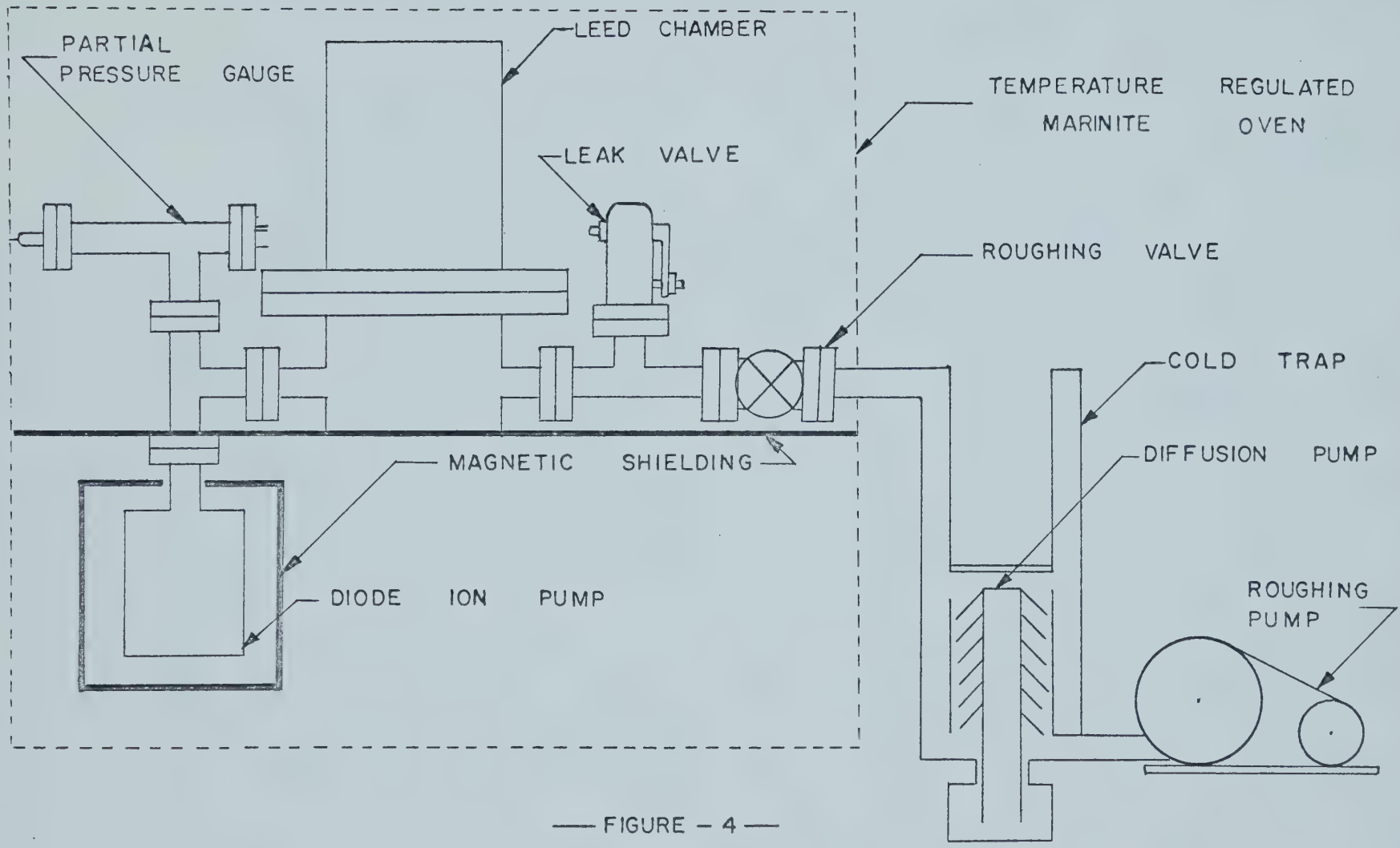

— FIGURE – 4 —

SCHEMATIC DIAGRAM OF EXPERIMENTAL APPARATUS

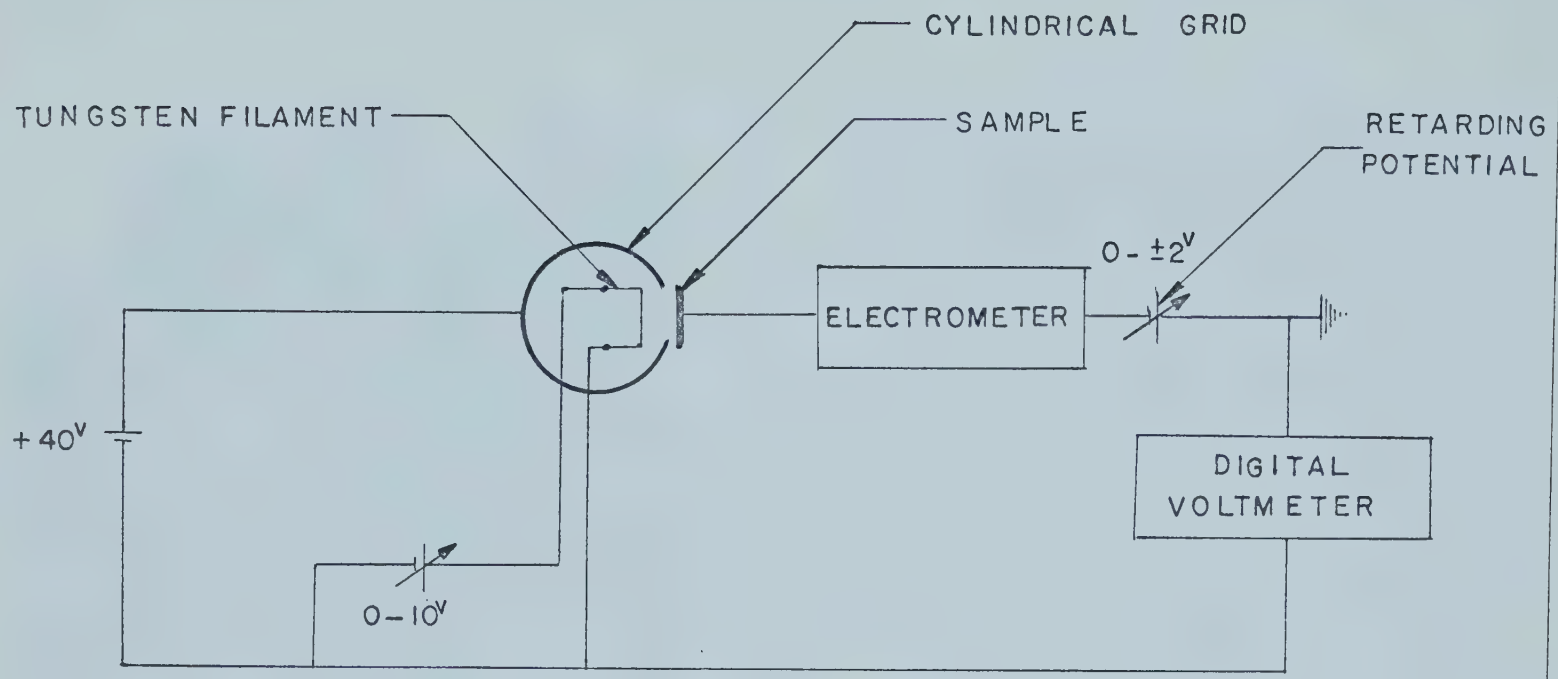

— FIGURE — 5 —

CIRCUIT FOR WORK FUNCTION MEASUREMENT

— FIGURE 6 —
(MAGNIFICATION = 200)
SPECIMEN BEFORE CLEANING

— FIGURE 7 —
(MAGNIFICATION = 200)
SPECIMEN AFTER CLEANING

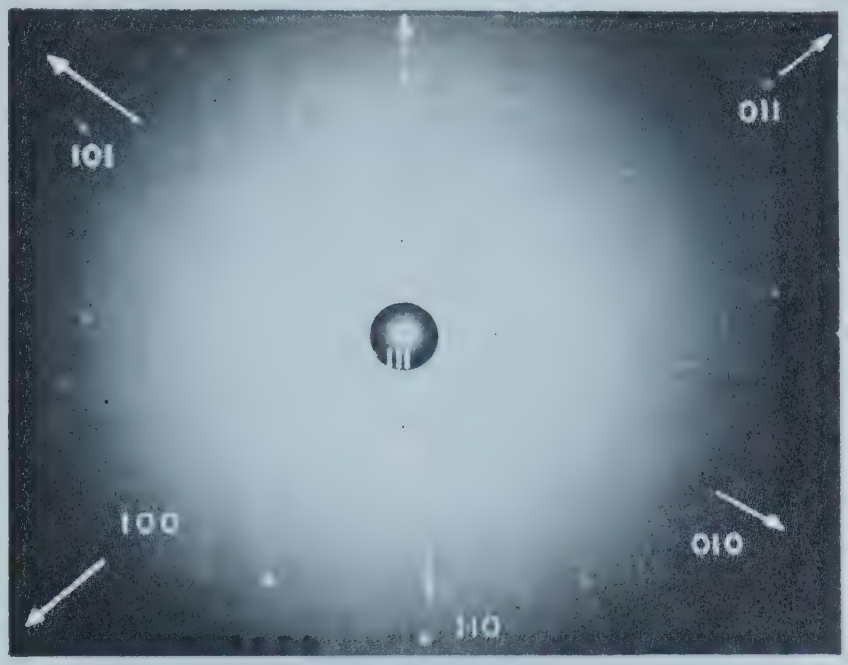

— FIGURE 8 —

LAUE BACK REFLECTION X-RAY

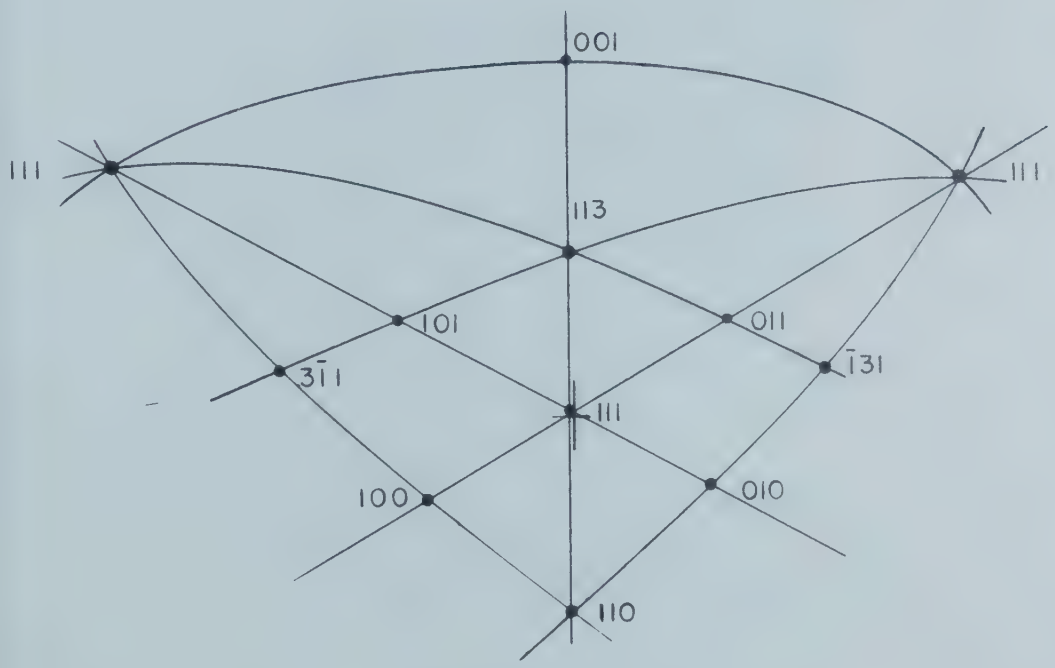

— FIGURE 9 —

STEREOGRAPHIC PROJECTION (111) PLANE

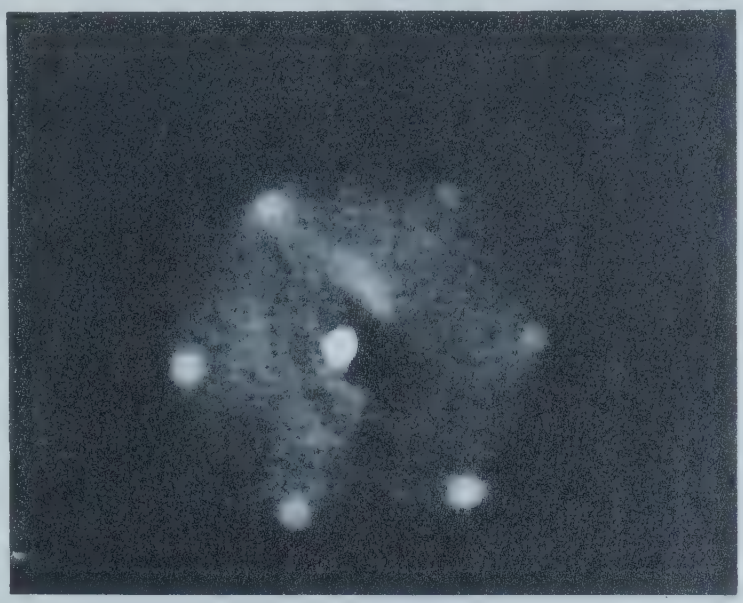

— FIGURE 10 —
BEAM VOLTAGE = 80 Volts
"LEED" PATTERN

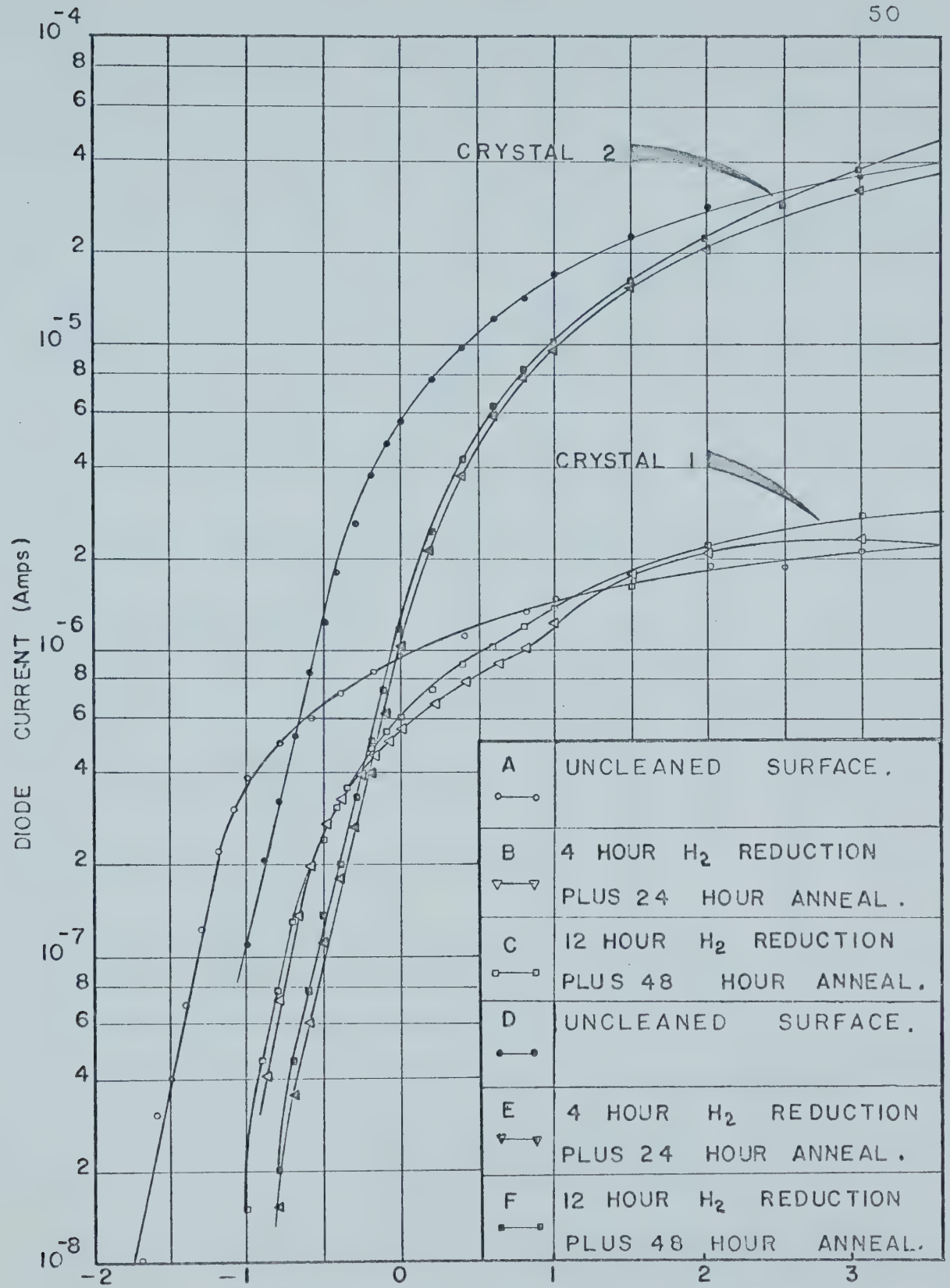

— FIGURE 11 —

RETARDING POTENTIAL FOR CRYSTAL CLEANING

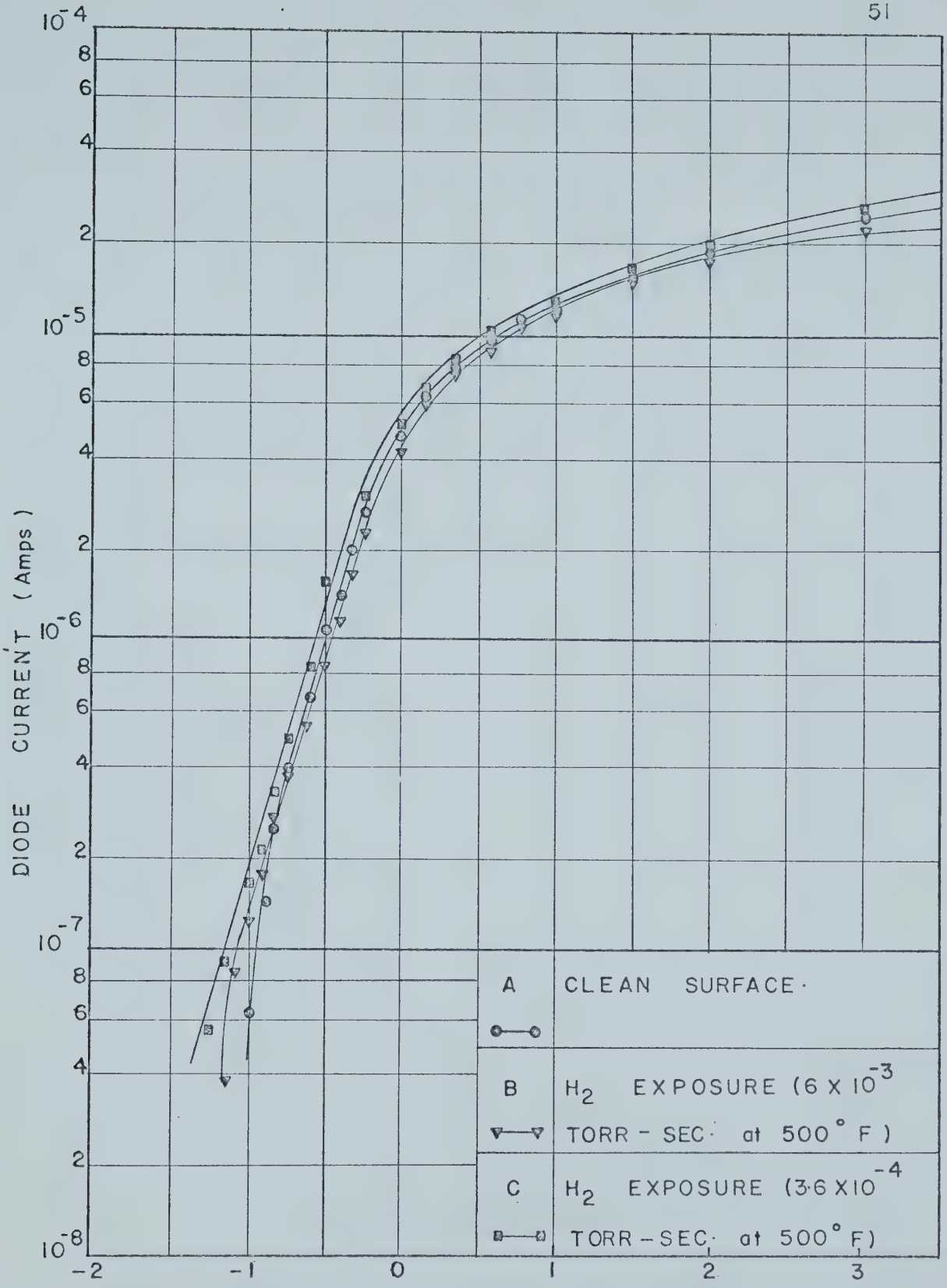

— FIGURE 12 —

RETARDING POTENTIAL FOR HYDROGEN EXPOSURE

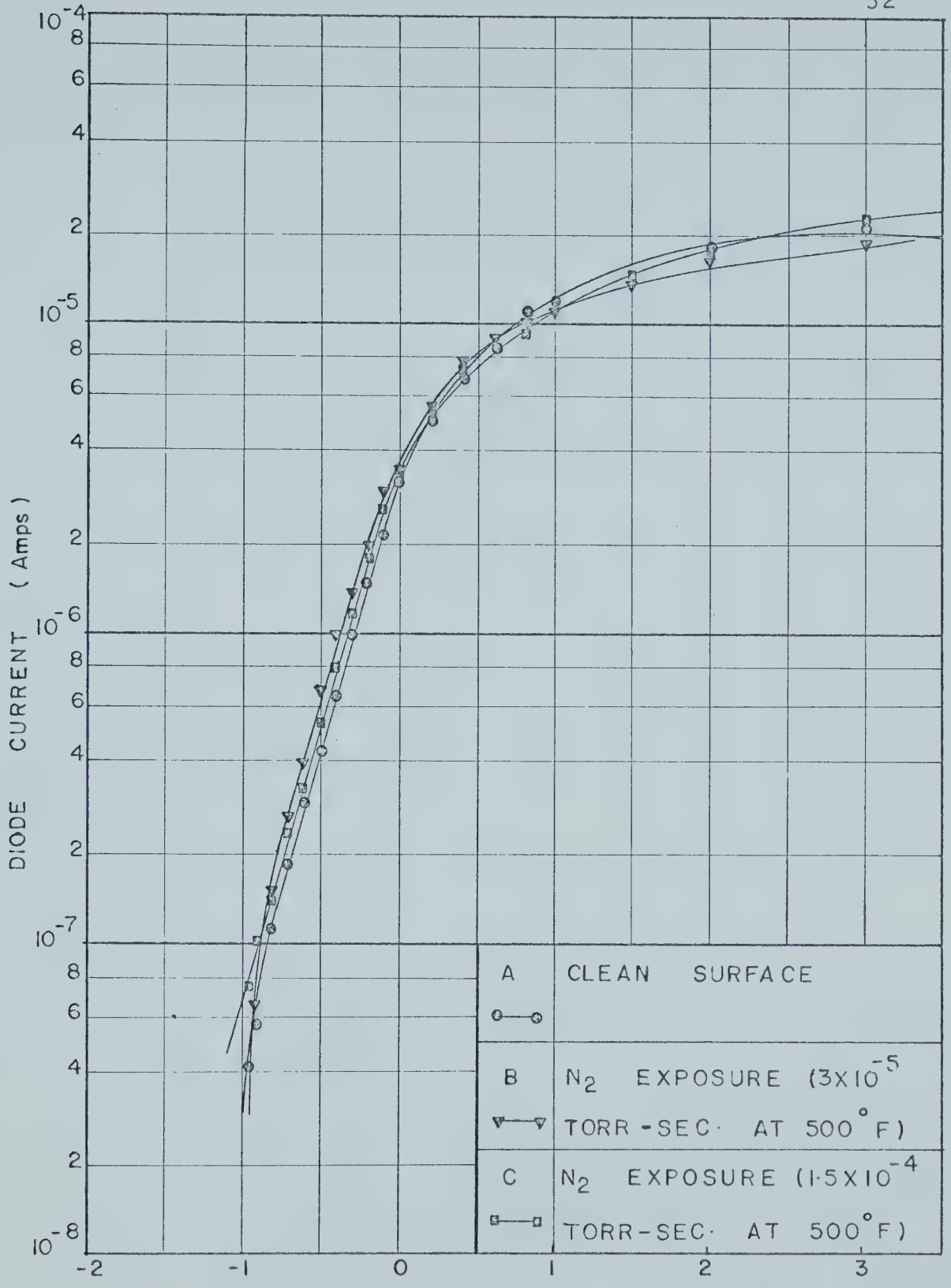

— FIGURE 13 —

RETARDING POTENTIAL FOR NITROGEN EXPOSURES

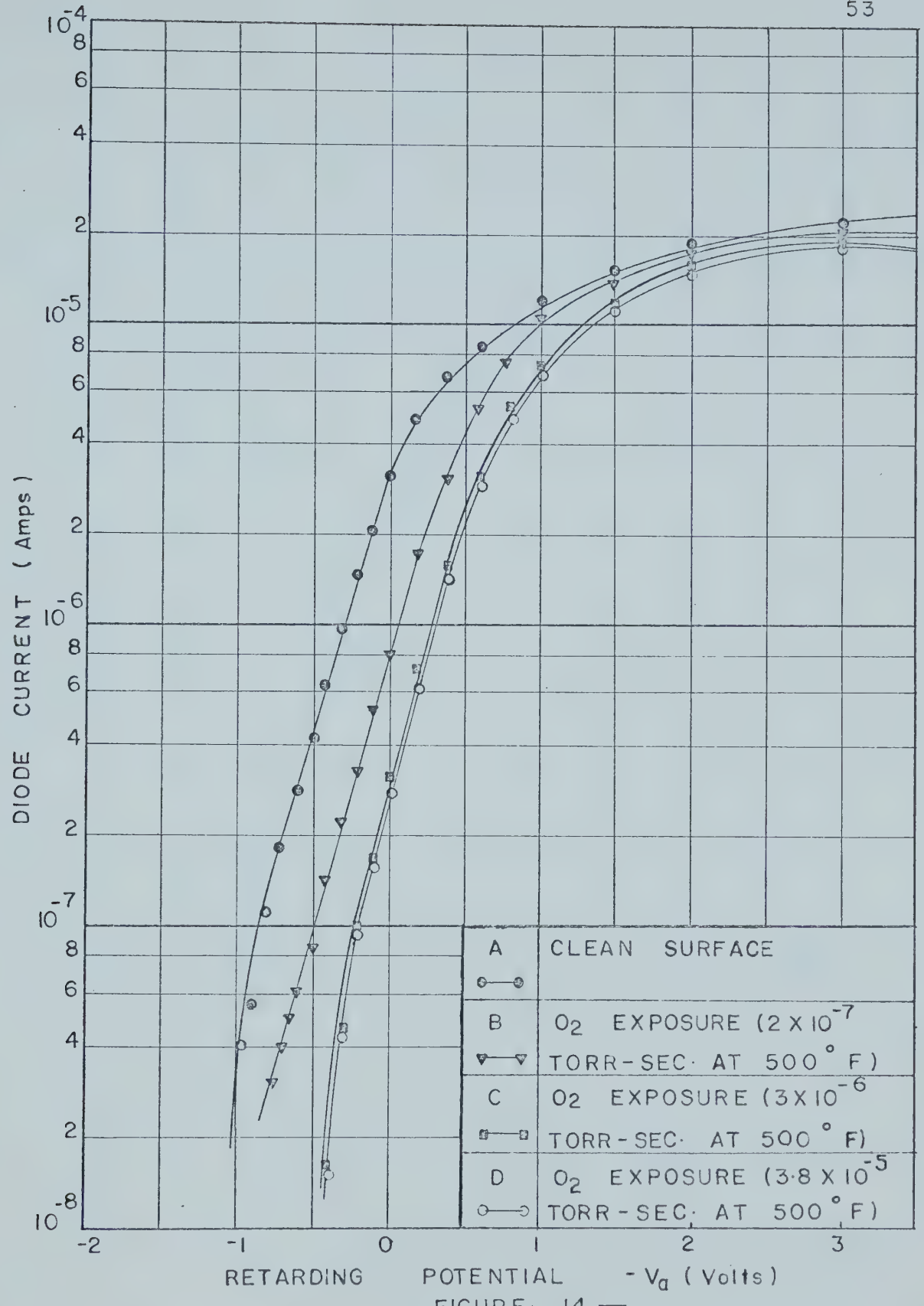

— FIGURE 14 —

RETARDING POTENTIAL FOR OXYGEN EXPOSURES

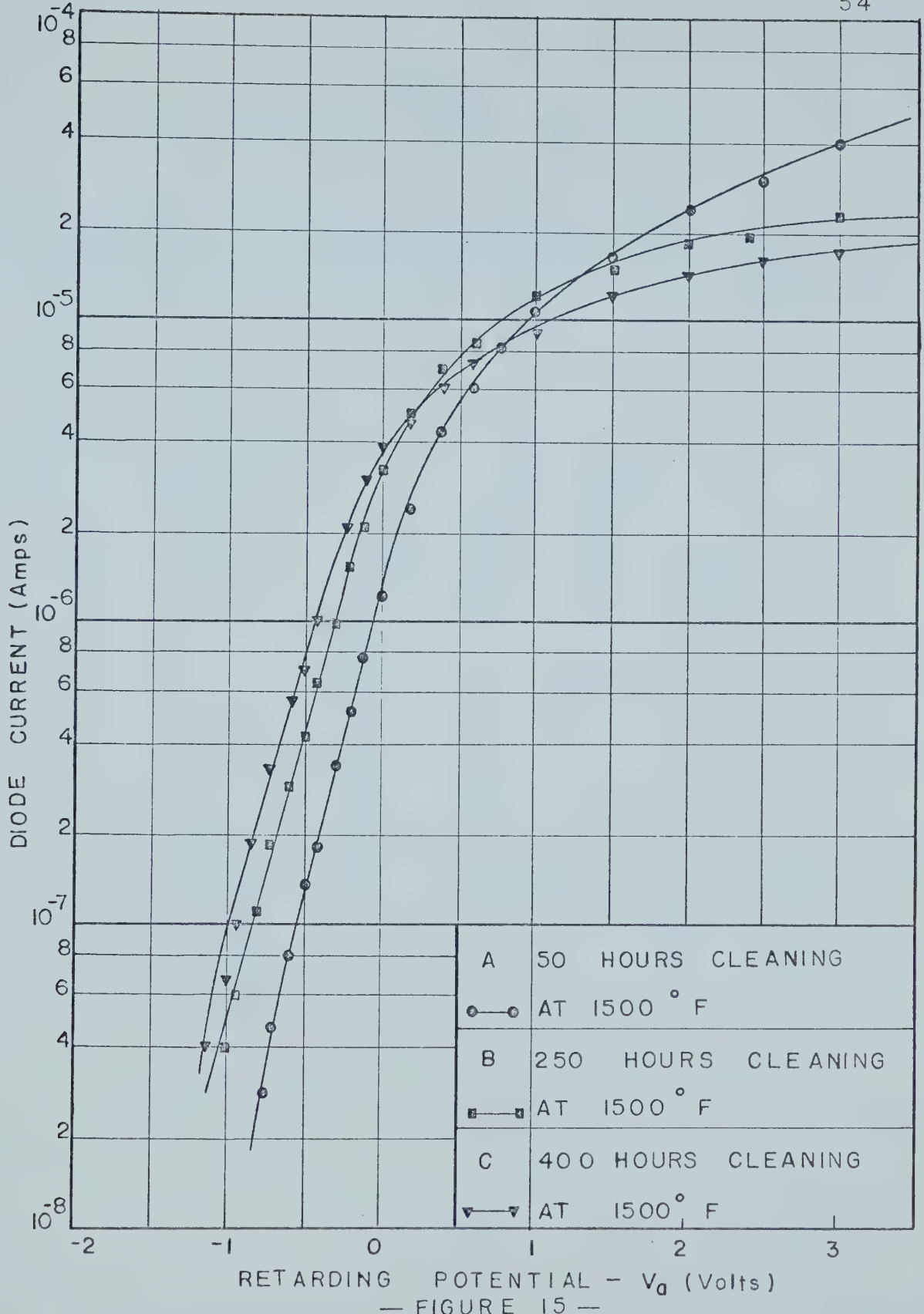

— FIGURE 15 —

RETARDING POTENTIAL FOR CLEAN SURFACE

TABLE I

RETARDING POTENTIAL DATA FOR CRYSTAL CLEANING

Ret. Voltage (Volts)	Diode Current (Amps x 10^7)					
	A	B	C	D	E	F
-1.7	.1					
-1.6	.3					
-1.5	.4					
-1.4	.7					
-1.3	1.25					
-1.2	2.20					
-1.1	3.0			.90		
-1.0	3.8		.15	1.25		
- .9		.40	.45	2.05		
- .8	5.0	.70	.75	3.2	0.15	0.20
- .7		1.3	1.3	5.2	0.35	0.45
- .6	6.0	1.9	2.0	8.4	0.60	.75
- .5		2.65	2.3	12.2	1.1	1.3
- .4	7.4	3.15	3.0	18.2	1.8	1.95
- .3		3.75	3.7	25.9	2.6	3.15
- .2	8.7	4.35	4.6	35.7	3.8	4.8
- .1		4.95	5.4	45.6	6.2	7.2
0	9.5	5.45	6.0	57	9.5	11.4
.2		6.55	7.4	77	21	23.5
.4	11.5	7.60	8.8	97	37.4	41
.6	12.5	8.75	10.0	117		61
.8	13.5	10.0	11.5	138	76	77
1	14.2	12.4	13.5	163	93	95
1.5	17		17	228	150	
2	18.5	19.6	20	276	200	200
3	23	23.5	26.5	342	320	295

TABLE II

RETARDING POTENTIAL DATA FOR HYDROGEN EXPOSURES

Ret. Voltage (Volts)	Diode Current (Amp x 10^7)			
	A	B	C	D*
-1.4				
-1.40				
-1.30				
-1.20				
-1.10		.35		.10
-1.00	0.60	0.65	0.55	.65
-0.9	1.40	1.45	1.35	1.30
-0.8	2.4	2.40	2.4	2.50
-0.7	3.75	3.5	3.7	3.6
-0.6	5.85	5.3	5.4	5.3
-0.5	8.9	7.75	8.5	8.0
-0.4	13.3	11.85	12.2	12.0
-0.3	18.8	16.7	18.6	17.4
-0.2	26.2	23.6	24.5	23
-0.1	35.1	32.0	34	32
00	45	42.5	45	43
0.2	64	61	63	62
0.4	81	77	80	78
0.6	96	92	95	93
0.8	110	106	105	107
1.0	126	120	120	120
1.5	162	155	155	150
2.0	196	190	195	190
3.0	245	235	250	230

D* Not plotted in figure 12

TABLE III

RETARDING POTENTIAL DATA FOR NITROGEN EXPOSURES

Ret. Voltage (Volts)	Diode Current (Amp x 10^7)			
	A	B	C	D*
-1.0				
-0.95		.40	.75	.86
-0.90		.55	1.0	1.0
-0.80	1.5	1.2	1.5	1.3
-0.70	2.0	2.0	2.2	2.0
-0.60	3.9	3.2	3.2	3.2
-0.50	6.6	5.0	5.25	4.8
-0.40	10.0	7.3	8.0	7.4
-0.30	13.6	11.8	12.2	
-0.20	20	17	17.8	16.4
-0.10	29	24		
0	34	35	34.5	34.2
0.2	55	54	54	54
0.4	74	72	70	70
0.6	88	86	84.5	88
0.8	105	100	99	99
1.0	116	116	115	126
1.5	140	146		140
2.0	159	177	160	168
3.0	198	235	200	206

D* Not plotted in figure (13)

TABLE IV

RETARDING POTENTIAL DATA FOR OXYGEN EXPOSURE

Ret. Voltage (Volts)	Diode Current (Amp x 10^7)		
	A	B	C
-1.0	.40		
-0.9	.55		
-0.8	1.1		
-0.7	1.8	.40	
-0.6	2.8	.60	
-0.5	4.2	.85	
-0.4	6.3	1.4	0.16
-0.3	9.7	2.2	.60
-0.2	14.6	3.3	.90
-0.1	21	5.2	1.4
0	31	8.0	2.5
.1			
.2	49	17.5	5.8
.4	68	32	14
.6	85	53	27
.8	102	76.5	47
1.0	117	100	67
1.2			86
1.4			104
1.6			120
1.8			100
2.0	180	185	175
3.0	210	200	202

APPENDIX I

CLEANING OF TYPE 304 STAINLESS STEEL

1. Electrolytic polish for 30 minutes in a bath of glycerine and phosphoric acid. Current density was set at 75 - 150 Amp/ft^2.
2. Steam.
3. Wash with acetone.
4. Wash with isopropyl alcohol.
5. Wash with methanol.
6. Rinse with distilled water.
7. Dry

APPENDIX II

CENTRE LINE AVERAGE

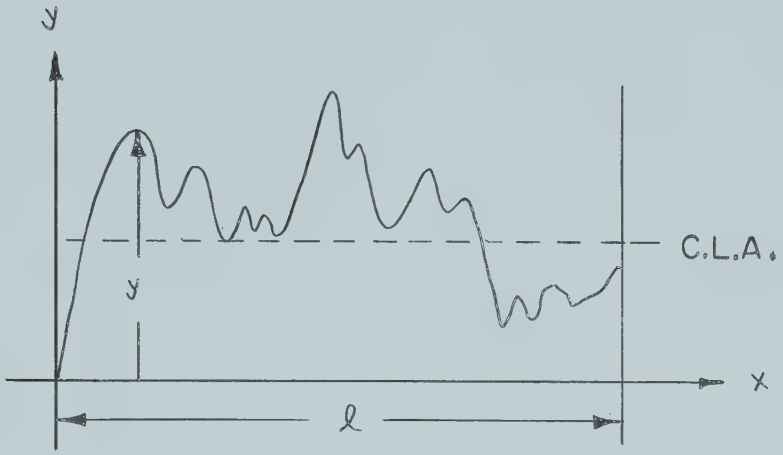

Centre line average = $\frac{1}{\ell}\int_0^{\ell} |y|\,dx$

(C.L.A.)

ℓ = length of distance on surface over which the averaging process is carried out.

B29918